

## 19. TURBIDITES AND TERRIGENOUS MUDS, DSDP LEG 25

Casey Moore, Earth Sciences Board, University of California, Santa Cruz, Santa Cruz, California

### ABSTRACT

Turbidites and/or terrigenous muds were recovered from eight sites along the southeast African continental margin during Leg 25 of the Deep Sea Drilling Project. Although these terrigenous deposits do not show equivalent facies between adjacent basins, they can be subdivided broadly by lithology. Biogenic and volcanic graded beds occur at five sites, whereas laminites (contourites?) are present at two sites. The graded beds, usually less than 20 cm thick, range in age between Oligocene and Recent; the laminites are Late Cretaceous and Eocene. A Late Cretaceous turbidite sequence (with virtually every characteristic of an Alpine flysch) comprises a portion of the continental rise of the Somali Basin. Thick Eocene and Miocene massive sand units were cored from the Somali and Mozambique Abyssal plains.

Detailed grain-size analyses of the graded beds and massive sands indicate up to 20 percent matrix of apparently primary origin. A C-M diagram suggests deposition of the graded beds and some of the massive sands by turbidity currents. The C-M diagram further suggests that portions of the massive sands may have been moved by a traction current, possibly as a "bed load" below a turbid flow. Regardless of the depositional process, the massive sands were transported between 750 and 1770 km over slopes as gentle as 1:1000.

The silicate fraction of the massive sands, graded beds, and terrigenous muds indicates derivation from the crystalline basement of Africa with a minor volcanic contribution. Samples of the terrigenous muds from several sites are anomalously enriched in palygorskite, a possible volcanic alteration product.

The turbidites cored on Leg 25 fit an idealized sedimentary model of a rifted continental margin excepting where density currents were diverted from lateral to longitudinal flow by a microcontinental fragment.

### INTRODUCTION

The sedimentary deposits cored on Leg 25 provide one example of terrigenous sedimentation along a complexly rifted continental margin. In this paper, I specifically summarize the deep-sea terrigenous deposits, attempt to outline some of their topical problems, and briefly discuss their provenance and distribution patterns in the context of their tectonic framework. Density underflow deposits of all types (turbidites) and muds (locally mudstones) are primarily emphasized. I restrict my discussion to the relatively pure terrigenous muds, believed to represent the land-derived component of the hemipelagic mixtures. The abyssal Somali and Mozambique basins (Figure 1) adjacent to Africa include thick sequences of massive sand (Sites 240 and 248), whereas graded beds occur at most Sites (239, 240, 241, 248, 249) adjacent to the continental margin. A spectacular flysch sequence composes part of the continental rise bordering the Somali Basin. All sites with significant turbidity current deposits also include sections of relatively undiluted terrigenous mud.

The single most important source of data for this paper is the hole summary books to which all Leg 25 scientists contributed during shipboard investigations. The grain-size and carbon-carbonate analyses were completed by the Deep Sea Drilling Project laboratory, supervised by J. Bodie. The X-ray analyses were carried out by I. Zemmels and H. E. Cook at University of California, Riverside. Acknowledgement is made to the donors of the Petroleum Research Fund, American Chemical Society (Grant No. 2483-G3), and the University of California for partial support of this research. Thoughtful reviews by R. E. Garrison, G. B. Griggs, and I. Zemmels significantly improved this contribution.

### TURBIDITES

#### Main Sediment Types

The term turbidite is used herein to designate probable density underflow deposits of all types. Graded beds and massive ungraded sands are included under this heading. Laminites, closely associated with graded beds, are

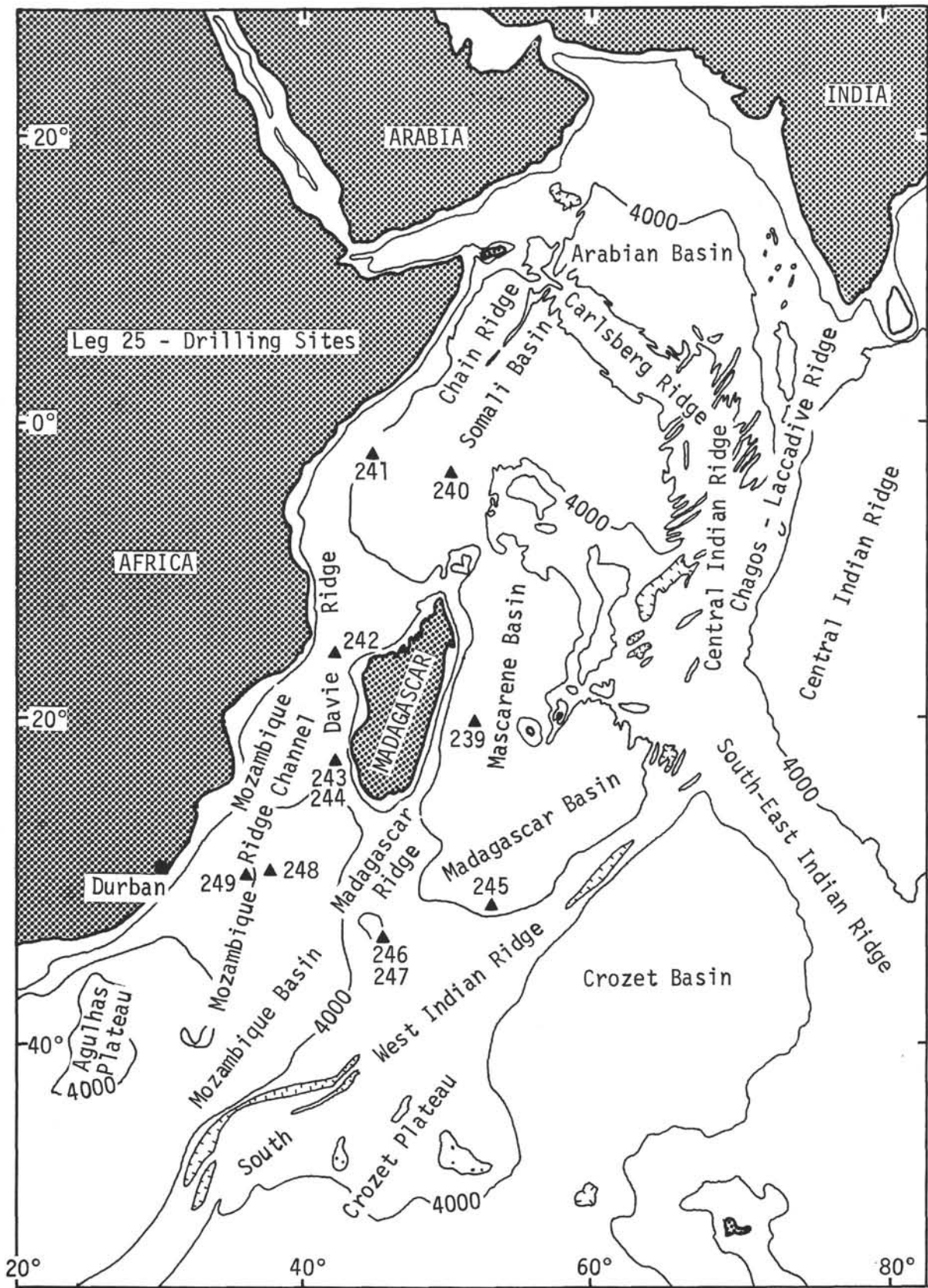


Figure 1. Location of Leg 25 drill sites and generalized bathymetry of western Indian Ocean.

discussed here though their mode of deposition remains uncertain.

The variety and distribution of turbidites discussed in this paper are based on shipboard visual examination of the cores. Only obvious examples are included; further detailed study may redefine and expand the classification and distribution of these deposits. Turbidites occur in cores from Sites 239, 240, 241, 243, 244, 248, and 249, spanning all major geologic time divisions from Cretaceous to Quaternary. They are subdivided into the following arbitrary headings: (1) graded beds, (2) massive sands, (3) laminites, and (4) flysch. The extraordinary flysch sequence cored at Site 241 is discussed separately even though it includes graded beds, massive sandstones, and laminites.

#### Graded Beds

Graded beds comprise a small but conspicuous portion of the cores from Sites 239, 240, 241, 248, and 249 (Plate 1). They are restricted to Quaternary age sediments at Sites 239, 240, and 248. Graded beds of Quaternary, Pliocene, Miocene, and possibly late Oligocene ages were penetrated at Site 241; however, those cored at Site 249 range from Aptian to Cenomanian. Neogene sediments cored at Site 241 are composed of 2-4 percent obviously graded beds; all other sites showed smaller percentages. Most graded beds measure 3 to 18 cm from base to top; however, several are at least 40 cm thick. Caution must be exercised in any interpretation of ages and distributions of graded beds since only obvious examples are discussed.

All graded beds from Sites 239 and 240, and most from 241, were composed of greater than 50 percent skeletal sand- and silt-sized grains. In contrast, volcanic detritus predominated in the graded beds cored at Site 249. These beds form a portion of a unit (287 to 352 m below the mudline; Cores 23-29) which consists primarily of volcanic siltstone with minor volcanic ash beds.

According to Barbara Zobel, most graded beds contain displaced and/or reworked fauna. Single beds from the Neogene sequence of Site 241 include benthonic foraminifera derived from inner shelf (nonreefal, <100 m depth), outer shelf, and abyssal environments. One middle Miocene bed at Site 241 contains reworked Eocene foraminifera.

#### Massive Sands

Thick massive sand sections were penetrated during drilling at Sites 240 and 248 (Plate 2). Surface samples of coarse sand were recovered from Sites 243 and 244 and will be considered with the massive sands. Abundant sand characterizes the interval from 148 to 195 meters below the mudline in the combined section of Holes 240 (Cores 4 and 5) and 240A (Cores 2 and 3). Most massive sands of Holes 240 and 240A are of early-middle to late Miocene age, though some are as old as early Eocene. No Oligocene massive sands were cored in Holes 240 and 240A. Massive sands at Site 248 are restricted to middle late Miocene, occurring from 130 to 274 meters below the mudline (Cores 4-9). The surface samples from Sites 243 and 244 contain Holocene foraminifera.

Drilling disturbance of the slightly cohesive sands hinders determination of textural and bedding properties. However, detailed examination of some unwashed sections indicates a slight upward size grading in sedimentation units at least 1 meter thick. The medium to coarse sand fraction comprises approximately 44 percent of the 7 meters of sediment recovered from the 18 meter penetration of Cores 4 and 5 of Hole 240. Recovery in Hole 240 and all other sand-rich sections was low, probably due to the slight cohesiveness of sand. If we assume that the voids noted in Cores 4 and 5, Hole 240 were represented by sand washed out during drilling, the apparent sand fraction of the 18 meter penetration rises to 77 percent. It is reasonable to assume that the massive sand units drilled on Leg 25 were originally composed of a much greater percentage of sand (75%?) than was actually recovered.

The microfauna of the massive sands is characterized by foraminifera derived from inner shelf and nearshore environments. At Site 240, Neogene foraminifera includes an abundance of mechanically resistant benthonic forms which are normally restricted to the reefal environment. Cores 8 and 9 (227 to 274 m) at Site 248 include large benthonic foraminifera characteristic of warm shallow water. A reworked pebble of Eocene age was noted in the surface sample from Site 243. In Hole 240A, Maestrichtian foraminifera occur in sands of early early Eocene age.

#### Flysch

Cores 25 to 29 (854 to 1174 m below the mudline) at Site 241 recovered an exceptional Turonian-early Senonian section of calcareous sandstone, graded beds, and fine laminite (Lombard, 1963) interbedded with claystone (Plate 3, Figures 1, 2, 4). This sequence accounts for 29 percent of the sediment penetrated at Site 241 and comprises a major sedimentary unit deposited in the early history of this rifted continental margin.

Individual calcarenites and calcareous sandstone beds range in thickness from 3 to 38 cm and represent 7 percent (by volume) of the recovered sediment. This figure is probably a maximum due to the preferential washing of less indurated claystones. Graded beds occur in thicknesses from a few millimeters to approximately 10 cm. Individual laminae averaging 2 mm thick comprise laminite units (Lombard, 1963) ranging from 1-3 cm thick.

The combination of rock types and conspicuous sedimentary structures (cross bedding, convolute lamination, slump structures, graded bedding, etc.) makes this sequence comparable in every way to classic flysch deposits (Dzulynski and Walton, 1965). The strong identity of these rocks may be, in part, due to the preservation and accentuation of the sedimentary structures during lithification. The term flysch is used explicitly to describe these cores (as distinct from other turbidites and terrigenous muds cored on Leg 25) in order to emphasize their similarity to flysch deposits of Alpine mountain belts.

The claystones are practically barren of foraminifera and only locally contain a sparse solution resistant nannoflora.

Apparently these rocks accumulated below the Turonian-early Senonian calcium carbonate compensation depth (CCD).

#### Laminites

In addition to those of the flysch (Site 241), well-developed laminites were recovered from Cores 10 to 13 (312 to 407 m below mudline) at Site 248 (Plate 3, Figure 3). These Eocene sediments are characterized by alternating thin laminae, several millimeters to several centimeters thick, predominantly of dark green and dark greenish gray color. Most laminae are composed of silt-bearing to silt-rich clay; local thin white laminae are made up of silt-sized carbonate grains (rhodochrosite). Volcanic ash may account for portions of the darker clay layers. The laminites are devoid of calcareous fossils but include well-preserved radiolarians and fish teeth.

#### Composition

The main sediment types can be clearly differentiated by their mineralogical characteristics which provide a basis for interpretation of provenance and some aspects of their depositional processes. Since Girdley and White (this volume) detail the mineralogy of the turbidite sands (including heavy minerals), the following discussion focuses broadly on the composition of the main sediment types. Vallier (this volume) treats the mineralogy of the volcanoclastic graded beds. The mineralogy of the laminites is not specifically covered below since those of Site 241 are discussed with the flysch and those of Site 248 under volcanoclastic sediments (Vallier, this volume).

#### Graded Beds

One of the most striking aspects of the graded beds at Sites 239, 240, 241, and 248 is the large quantity of biogenic detritus (Plate 4, Figures 1, 4, 5). This material ranges in abundance from 10 to 65 percent (avg. 50%) of the turbidite coarse fraction. Foraminifera (benthonic and planktonic) are predominant with lesser amounts of sponge spicules, Radiolaria, diatoms, and coccoliths. Pyrite occurs within foraminiferal tests (Plate 4, Figure 5) and sponge spicules and locally comprises a large proportion of the sediment of the matrix (Plate 4, Figure 1). Glauconite is present as individual grains or as pseudomorphs of foraminifera.

The graded beds include a terrigenous component composed mostly of quartz and potassium feldspar but with minor plagioclase. Virtually every thin section of graded beds from Sites 239, 240, 241, and 248 contained a small (<1%) but conspicuous amount of green hornblende (Plate 4, Figures 2, 3). Tourmaline and pink garnet occur locally.

Several graded beds cored from Site 249 are composed predominantly of volcanic glass (including shards and irregular blebs in various states of devitrification) and plagioclase laths. These rocks also include glauconite and foraminiferal tests. Secondary calcite accounts for the lithification of these volcanic graded beds.

#### Massive Sands

In contrast to the graded beds, the massive sands are primarily composed of detrital quartz and feldspar (Plate 5). Quartz plus orthoclase ranges from 60 to 80 percent; whereas, microcline plus plagioclase may vary from less than 10 to 30 percent. Granitic rock fragments and composite quartz grains occur locally (Plate 5, Figures 3, 4). Most thin sections contain green hornblende, which locally comprises up to 2 percent of the sample. Other heavy minerals include pink garnet, zircon, orthopyroxene, hematite, and magnetite(?). Thin section observations indicate 0-15 percent primary clay matrix (Plate 5, Figure 1) (also see grain-size analyses). Biogenic detritus comprises less than 5 percent of the massive sands.

In summary, the massive sands are enriched in silicate minerals relative to the graded beds but both contain similar compositional components.

#### Flysch

The massive and graded beds, and laminites of the flysch at Site 241, contain identical minerals but in variable proportions. On the average, sand-sized detritus is composed of 50 percent silicate grains and 50 percent carbonate grains. The silicate fraction is predominantly quartz and orthoclase with minor plagioclase and microcline; foraminifera and various shell fragments comprise the carbonate fraction. Chlorite, muscovite, and biotite are present, with the latter being most abundant; local concentrations (15%) of biotite occur in some distal graded beds. Green hornblende and pyrite account for <1 percent of the flysch sands. Elongate irregular pyrite concentrations (Plate 6, Figure 5) apparently replace fossil wood fragments. The carbonate and silicate grains are included in a micritic matrix which is locally neomorphically recrystallized (Plate 6, Figures 3, 4).

The composition of the flysch (Site 241) is similar to that of the graded beds (Sites 239, 240, 241, 248) since they both contain roughly equal amounts of silicate and biogenic detritus. However these units may be distinguished by individual components (e.g., large concentrations of mica in the flysch).

X-ray mineralogy serves to characterize the composition of the fine-grained portions of the flysch. A ternary plot of kaolinite + mica-montmorillonite + chlorite-palygorskite (Figure 2) shows that, with one exception, the fine-grained turbidite fraction and the associated terrigenous muds have a similar clay mineralogy. In both cases, the sediments are enriched in montmorillonite since chlorite is minor (<4%). Relative to the flysch, the younger muds from Site 241 contain less montmorillonite, apparently representing a secular, nondiagenetic variation to clay mineralogy.

Significantly, the X-ray data indicate that the fine-grained turbidity current deposits contain various amounts of carbonate minerals, whereas the associated terrigenous muds are barren of calcite (Figure 3). This fact suggests that the carbonate-bearing turbidites were deposited instantaneously below the prevailing Turonian-early Senonian CCD. Thus, the carbonate detritus in the rapidly deposited

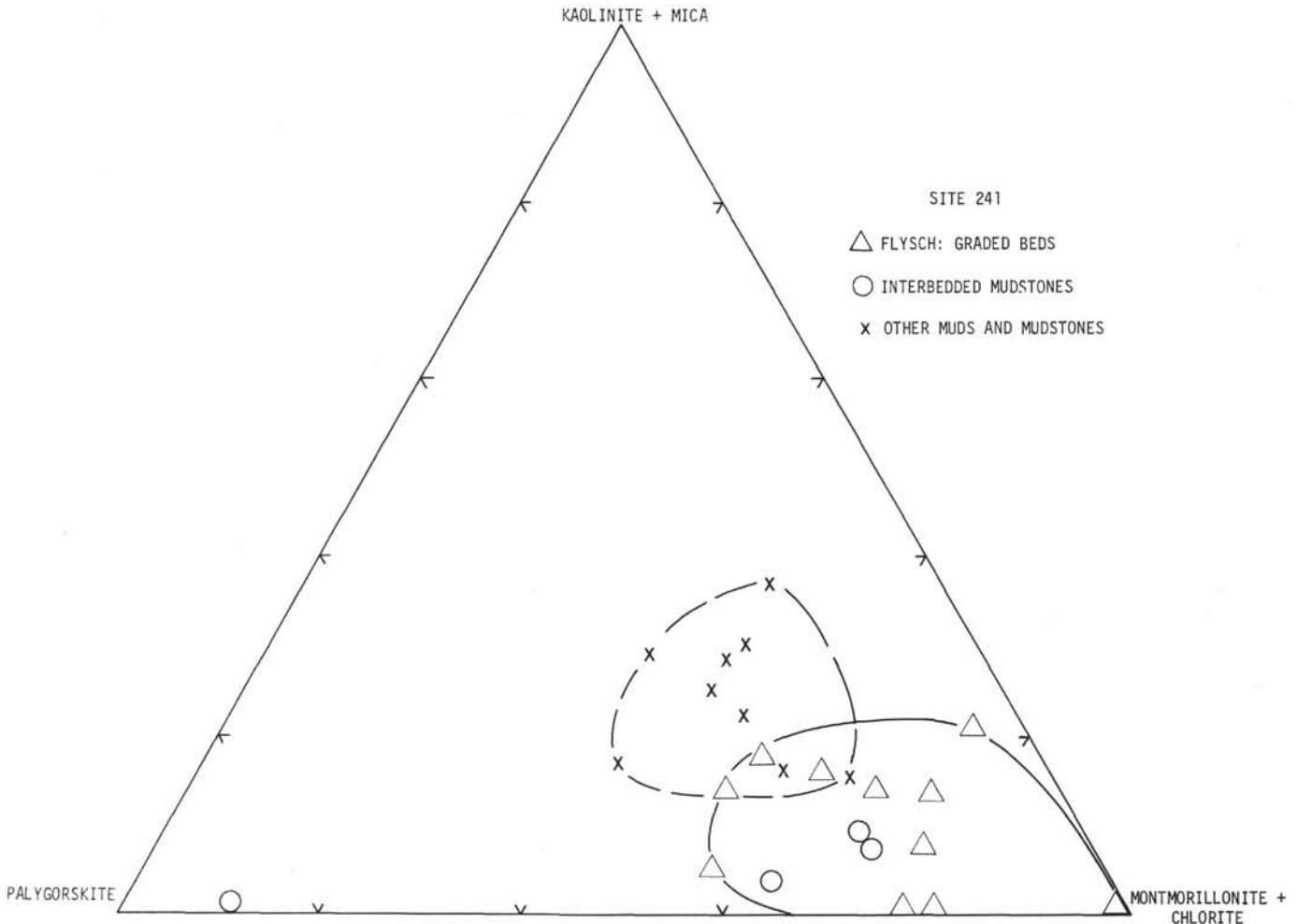


Figure 2. Ternary plot of X-ray clay mineralogy ( $< 2\mu$  fraction) of flysch (graded beds and interbedded mudstones) and other terrigenous muds and mudstones, Site 241 (data from Matti *et al.*, this volume). Note that, with one exception, the clay mineralogy of the turbidites and interbedded mudstones is similar, but apparently significantly different from other (younger) terrigenous muds cored at Site 241.

turbidites was shielded from solution, whereas carbonate material, settling slowly from the water column, was dissolved in transit or on the sea floor preceding burial. Scholle (1971) has similarly interpreted an Upper Cretaceous carbonate turbidite sequence in the northern Apennines, Italy.

The basal silt and silty clay of the laminites of Site 241 are comprised of 10-60 percent quartz and feldspar, 30-90 percent carbonate, and approximately 10 percent clay. The carbonate fraction is predominantly biogenic, though varying amounts of unidentifiable carbonate fragments are present. Overall, the laminites are mineralogically similar to the graded beds with the flysch sequence of Site 241.

## Texture

### General Observations

All mechanical grain-size analyses of turbidites cored on Leg 25 are compiled in Figure 4. The analyses represent samples taken near the bases of the graded beds but at

various intervals in the ungraded, massive sands. The massive beds are composed mostly of sand, always with less than 20 percent clay and up to 43 percent silt. Significant textural overlap occurs between the massive sands and graded beds which contain up to 69 percent sand. The broad textural dispersion of the graded beds reflects sampling of basal layers ranging through the Bouma A-D sequence. The finest basal grain sizes occur in graded beds from the flysch (Site 241). This fact is probably a function of sampling since diagenesis and minor drilling deformation permitted the recognition of fine-grained, subtly graded beds in the lithified flysch.

### Detailed Grain-Size Analyses

Quantitative grain-size determinations aid in classifying and interpreting the depositional processes of the turbidites cored on Leg 25. Twenty-three detailed grain-size analyses (completed by the DSDP Shore Laboratory) provide the basis for the following discussion. The analyses are at one

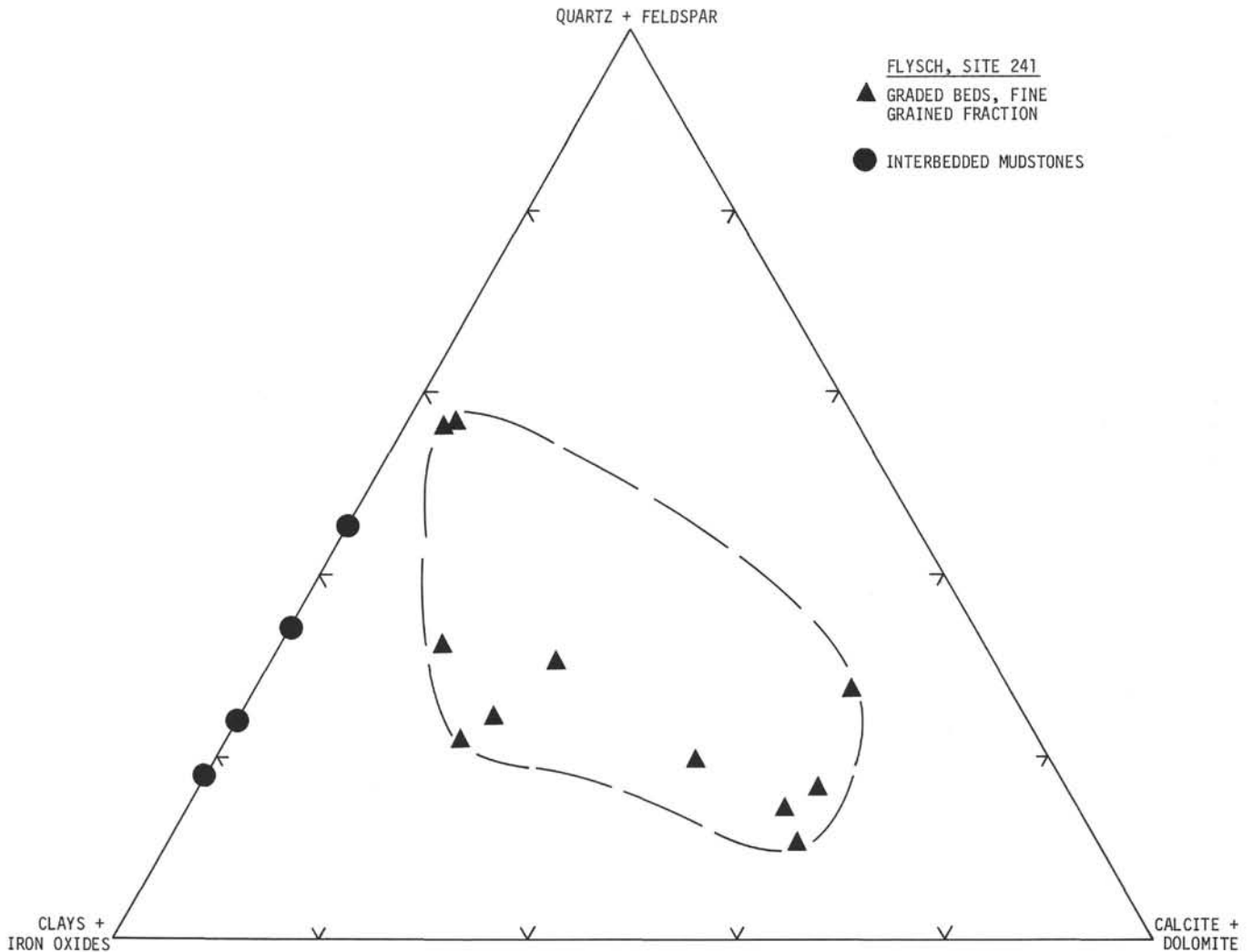


Figure 3. Ternary plot of bulk X-ray mineralogy from fine-grained portions of flysch sequence, Site 241 (data from Matti *et al.*, this volume). Note that interbedded (homogenous) mudstones are barren of calcite and dolomite, whereas the graded beds include variable amounts of carbonate minerals.

phi intervals for sizes of less than zero and greater than four phi, but at quarter phi intervals from zero to four phi. Time limitations have prevented investigation of many textural parameters which can be derived from the cumulative curves plotted below. The data from which these diagrams were generated are presented by White (this volume).

#### Cumulative Frequency Curves

The grain-size data are represented as cumulative curves since all statistical parameters can be read directly from this plot. Figures 5, 6, and 7 summarize the cumulative curves for graded beds, massive sands, and flysch.

Excepting one anomalous curve (Figure 5), the graded beds exhibit a bimodal grain-size distribution with the major mode between 3 and 5  $\phi$  (very fine sand to coarse silt). The minor mode is composed of sediment finer than 10  $\phi$  (clay), which accounts for 5-20 percent of the graded beds. Thin section observations reveal no diagenetic alterations which could have formed this fine matrix; apparently the clay-size mode is a primary depositional feature.

Cumulative frequency curves of the massive sands (Figure 6) show a bimodal grain-size distribution similar to that observed in the graded beds. The major mode occurs between 0 and 4  $\phi$  (coarse to very fine sand) with the minor mode comprised of material finer than 10  $\phi$  (clay). The clay fraction accounts for up to 15 percent of the massive sands and apparently is of primary origin.

The degree to which unconsolidated sands are "washed" by drilling fluid during coring will effect their grain-size distribution. Figure 8 illustrates cumulative curves of sands which, based on microscopic textural observations, appear unwashed. Three cumulative curves from lower, middle, and upper portions of a one-meter-thick massive sand are plotted in Figure 9. This massive sand interbedded between mud sequences macroscopically appears unwashed. Thin sections from the lower and middle portions of this massive sand show little or no matrix, whereas, the top of the massive sand includes 12 percent clay matrix. Is the lack of matrix in the lower and middle portions of this bed due to selective washing or enhancement of sorting by the

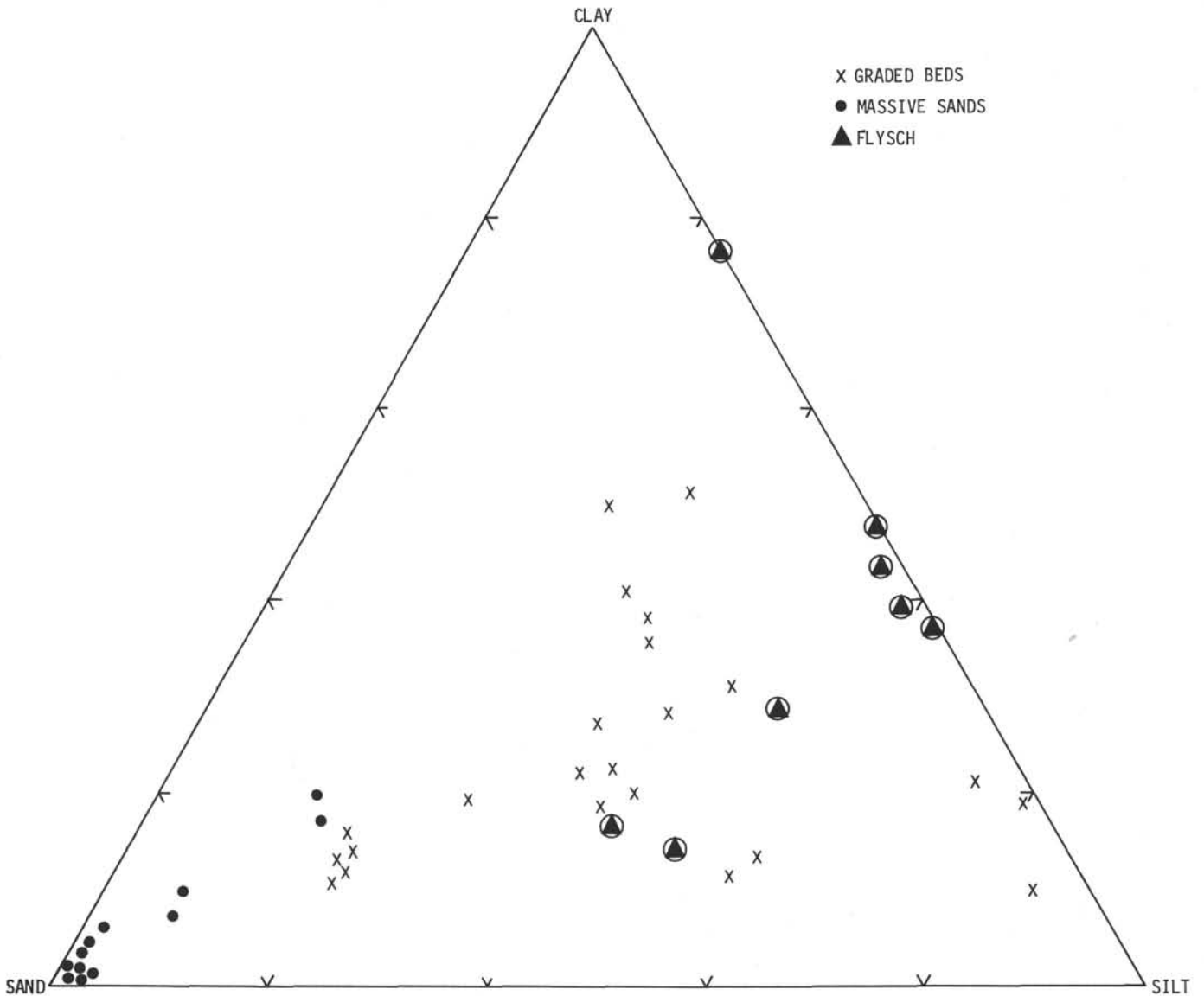


Figure 4. *Texture of turbidites; analyses from basal portions of graded beds but various levels in massive sands. With one exception all textural analyses of turbidites from the flysch are basal portions of graded beds.*

depositional process? I can only conclude that caution must be used in interpreting some grain-size analyses of these massive sands.

The flysch (Site 241) includes massive sandstone and graded beds which range in grain size from predominantly fine sand-coarse silt to clay (Figure 7). The coarsest analysis (Figure 7, curve 1) was taken from a massive sandstone 37 cm thick (Plate 7, Figure 1). The finest basal sample (Figure 7, curve 7) macroscopically shows grading only defined by color; however, a second grain-size analysis at the top of this bed confirmed size grading. As the medium grain sizes of the flysch turbidites increase, so does the tendency towards sharply defined bimodality (Figure 7). This trend is also shown in a comparison of the cumulative curves for graded beds and massive sands (Figures 5, 6). Apparently, as the energy of the turbidity flow increases, the processes responsible for transporting the coarser sediment becomes more sharply defined. Calcareous sandstone and siltstone layers of the flysch sequence were strongly lithified and not amenable to mechanical size analysis. Visual inspection

suggests their grain size is similar to the massive sandstone represented by curve 1, Figure 7.

#### *C-M Plot*

The main purpose of detailed textural analysis is to determine depositional processes. Binary plots of the size of the coarsest one percentile ( $C$ ) versus the size of the median ( $M$ ) of a suite of samples often defines graphic patterns characteristic of specific depositional environments (Passega, 1957, 1964). A  $C-M$  diagram (Figure 10A) has been generated from the detailed grain-size analyses of all graded beds and massive sands (including those from the flysch, Site 241). In general, the analyses define a trend parallel to the line  $C=M$ , but with a sharp increase in  $C$  relative to  $M$  for the coarser samples. Note that a gradation occurs between analyses taken from A-Bouma intervals (graded beds) and the massive sands. Also a crude gradation from A-D Bouma intervals occurs from coarser to finer along the major trend parallel to  $C=M$ .

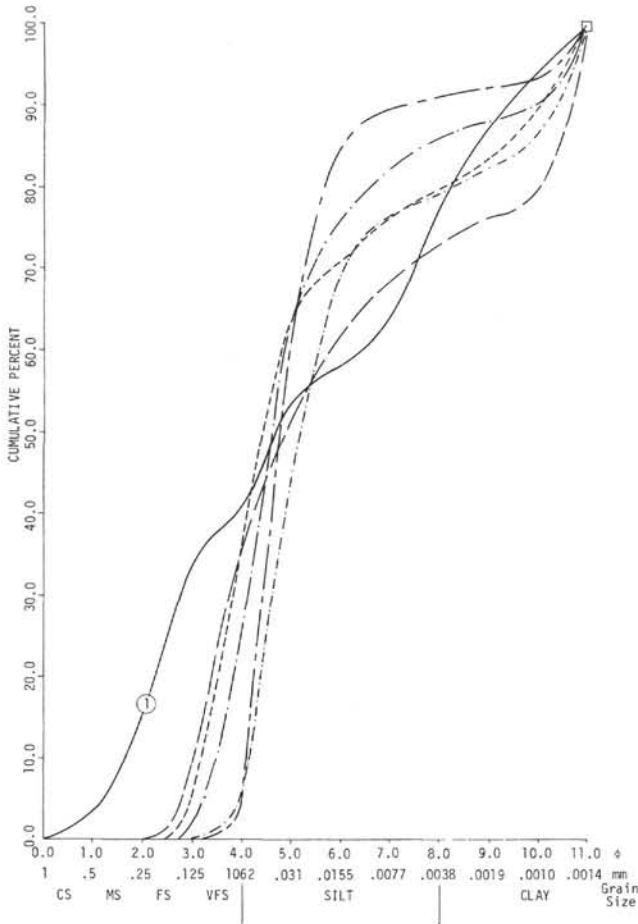


Figure 5. Cumulative frequency curves of graded beds cored at Sites 230, 240, 241 (exclusive of flysch). Note anomalous curve 1.

**Sedimentary Structures**

The sedimentary structures noted during shipboard description of turbidites are summarized in Table 1. Graded bedding was most frequently observed, followed in abundance by massive bedding and cross-bedding. The flysch from Site 241 shows the most prolific suite of sedimentary structures. The visibility of these features was enhanced by diagenesis and minor drilling deformation.

The sedimentary structures of the turbidites may be conveniently discussed in relation to their positions in the Bouma A-E intervals. Massive (Bouma A interval) characterized many basal layers of graded beds as well as the massive sands. Numerous examples of cross-bedding and convolute lamination (Bouma C interval) are present; these structures are particularly well represented in the lithified calcareous sandstones of the flysch of Site 241 (Plate 8, Figure 1, 4). Convolute lamination, diagnostic of subaerially exposed turbidites, is rarely recovered in deep-sea cores but convincingly preserved in the flysch. The upper interval of parallel lamination (Bouma D interval) occurs both within and at the base of graded beds (Plate 7, Figures 2, 3). In both cases, this structure is topped by homogenous fine-grained sediment (Bouma E interval).

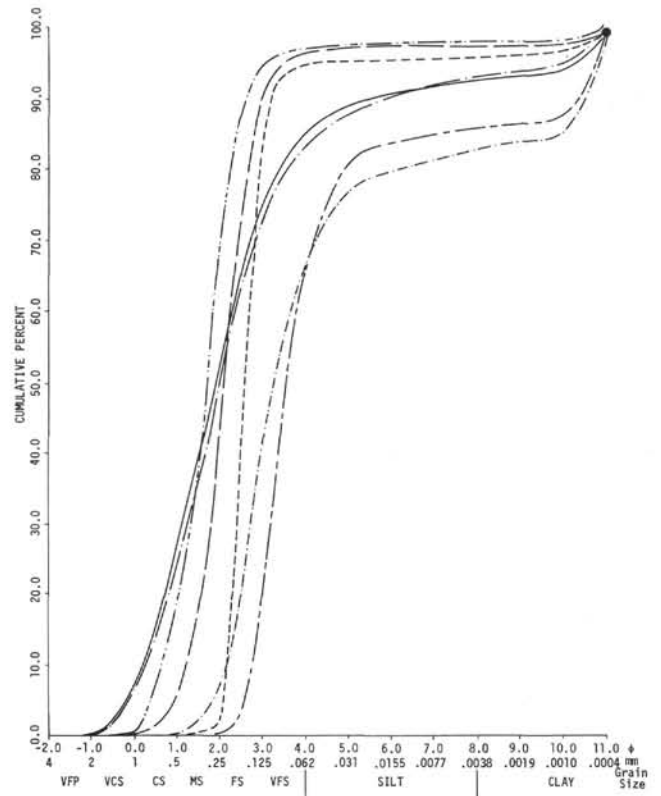


Figure 6. Summary cumulative frequency curves for massive sands of Sites 240 and 248.

**TABLE 1**  
Inventory of Sedimentary Structures, Leg 25

Structure	239	240-A	241	243-4	248	249
Graded Bedding	X	X	X		X	X
Massive Bedding		X	X	?	X	
Cross Bedding			X		X	X
Convolute Lamination			X			?
Slump Folds			X		X	X
Rip-up Clasts			X			
Burrowing			X		X	
Laminites			X		X	
Sole Marks			?			?
Load Clasts			?			?

Other conspicuous sedimentary structures include slump folds and sole marks. A superbly developed slump fold occurs within the flysch at Site 241 (Plate 8, Figure 3). Detailed inspection of this fold suggests it caused (or was caused by) a density flow since it passes smoothly upward

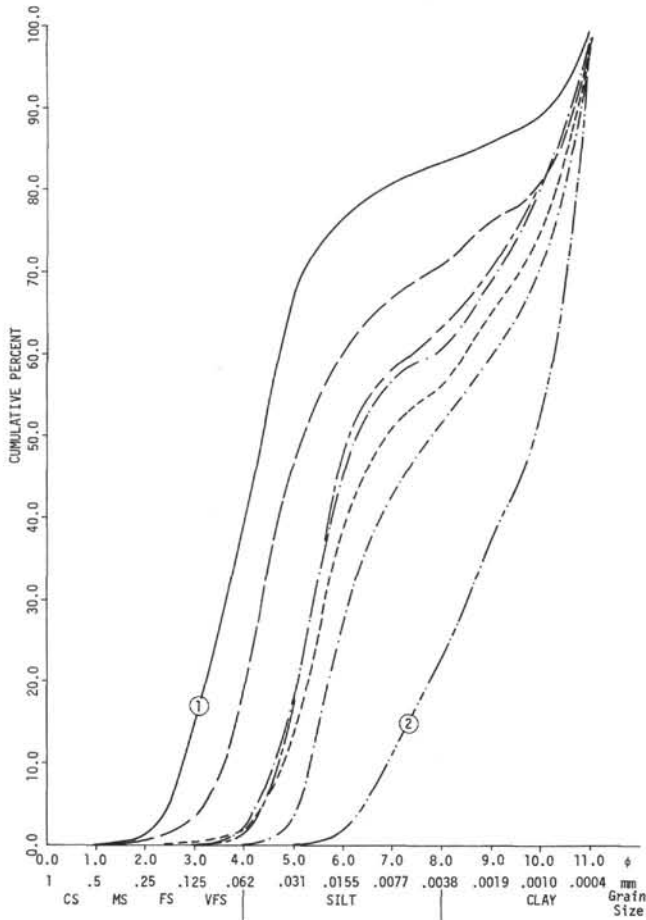


Figure 7. Cumulative frequency curves for flysch, Site 241. Curve 1 from basal sample of massive sand illustrated Plate 4, Figure 1. Curve 2 from base of distal graded bed which macroscopically shows only color grading (textural analyses verify size grading).

into a graded bed. The lower limb of this fold remarkably preserves overturned cross-beds. Local abundance of rip-up clasts (Plate 7, Figure 1) reflect erosion of substrata by the turbidity currents. At least one example of an erosional sole mark is present (Plate 3, Figure 4).

The laminites of Sites 241 and 248 show fine laminae ranging from less than 1 mm to greater than 1 cm. Individual layers may be ungraded, graded, reverse graded, or subtly cross laminated (Plate 3).

### Diagenesis

Cores obtained by deep-sea drilling are ideal subjects for diagenetic studies since their age and depth of burial are well known. The Leg 25 turbidites illustrate several diagenetic phenomena including formation of pyrite, dolomite, and neomorphic calcite, and the solution of silicate minerals.

Pyrite is one of the most widely observed diagenetic minerals. Generally, pyrite occurs in likely sites high in organic matter content—within foraminifera tests (Plate 1, Figure 5), sponge spicules, or pseudomorphing apparent wood fragments. Pyrite is developed in turbidites as young as Pleistocene and is present in most older beds. Apparently, iron sulfide minerals formed through bacterial

reduction of sulfate to sulphide which then combined with dissolved ferrous iron (Berner, 1971). The less stable iron sulfide minerals were then diagenetically transformed to pyrite (Berner, 1971).

All stages of compaction and lithification occur within the turbidites. Although many vary from unconsolidated to semiconsolidated, some are highly lithified, apparently as a result of recrystallization or replacement of calcium carbonate. At Site 239, calcareous detritus from a turbidite bed is replaced by gypsum forming a thin lithified unit at a depth of 158 meters. At Site 249 (284 m), graded beds are well lithified due to replacement of volcanoclastic detritus by calcium carbonate.

The calcareous sandstones of the flysch (Site 241) may be either strongly cemented by neomorphic calcite or semiconsolidated by a compacted micrite. In the latter case, abundant pyrite locally pseudomorphs apparent wood fragments (Plate 6, Figure 5). Within the highly lithified sandstones, quartz and potassium feldspar are replaced along their grain boundaries by dolomite. The organic carbon content of three semilithified and seven lithified sandstone averages 0.9 and 0.13 percent, respectively, indicating that the pyritization process did not completely oxidize the organic matter in the semilithified (originally carbonaceous) sandstones. The replacement of quartz by dolomite in the lithified sandstone suggests a basic pH, whereas the pyritization of organic matter indicates reducing conditions in the semilithified sandstones. The lack of both well-developed calcite cement and secondary dolomite seems to show a positive correlation with high organic carbon content. Possibly, the formation of an organic grain coating prevented recrystallization and replacement of detrital material (Bathurst, 1971, p. 252-254).

The fine-grained matrix component of the massive sands is not a diagenetic product, a point worthy of special reiteration in light of the emphasis placed by Cummins (1962) and subsequent workers on the secondary origin of greywacke matrix. The massive sands are always unconsolidated and never buried more than 300 meters. The massive sands nowhere contain unstable lithic fragments, either because they were initially absent or subsequently completely altered. Since it is surmised that neither the over burden pressures nor temperatures at these shallow depths would be sufficient to transform unstable lithic fragments to matrix, the matrix must be a primary sedimentary deposit.

### Depositional Processes

#### Graded Beds

The graded beds, with their sharp bases, gradational tops, cross-bedding, convolute lamination, and displaced fauna, can be reasonably interpreted as the deposits of turbidity currents (Kuenen, 1964). Moreover, the orderly development of the Bouma sequence (intervals A-E, up section) is hydrodynamically consistent with the deposition of the graded beds during a waning flow regime (Walker, 1965). In contrast to the graded beds, the massive sands and laminites, obviously, cannot be interpreted as the deposits of turbidity currents.

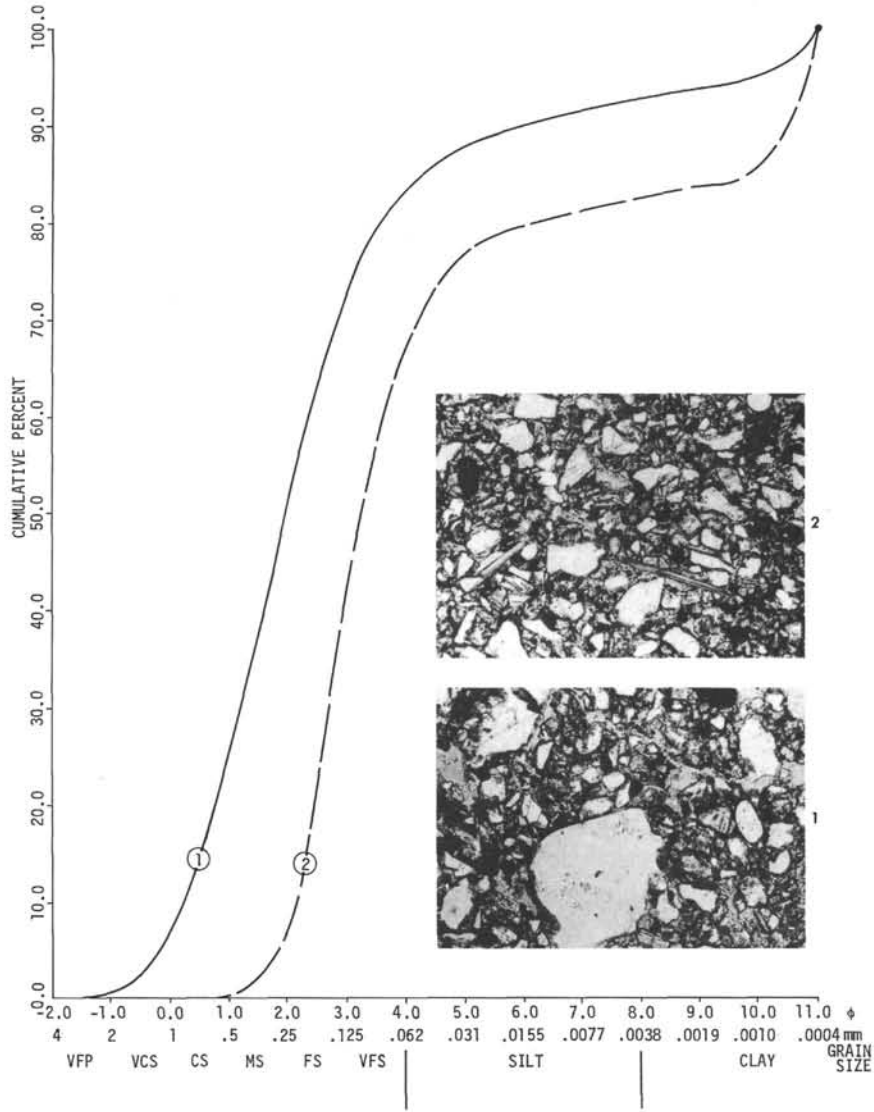


Figure 8. Textural properties of massive sand samples (one from 240-5-6, 136 cm; two from 248-6-1, 146 cm). The preservation of fine-grained matrix between the sand and silt grains indicates a lack of washing. Note that mode in sand-sized particles is less pronounced (less steep) than the similar mode in possibly washed sands (Figure 9). Width of photomicrograph approximately 3 mm.

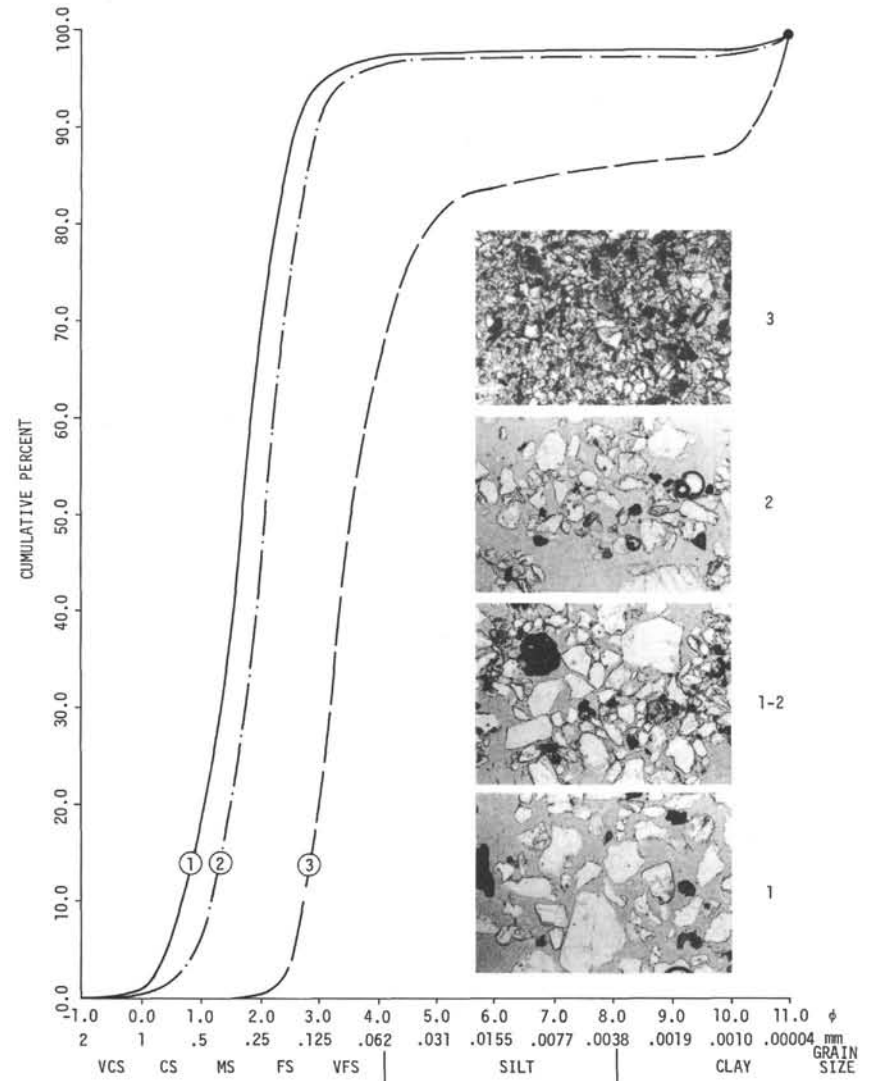


Figure 9. Textural properties of massive sand approximately one meter thick (240-4-2-21, 125 cm). Curves 1, 2, and 3, from 123 cm, 79 cm, 21 cm, respectively; photographs 1, 1-2, 2, 3 from 123, 100, 79, and 21 cm, respectively. Grading apparently more pronounced in upper half of massive bed. Width of photomicrograph approximately 3.5 mm.

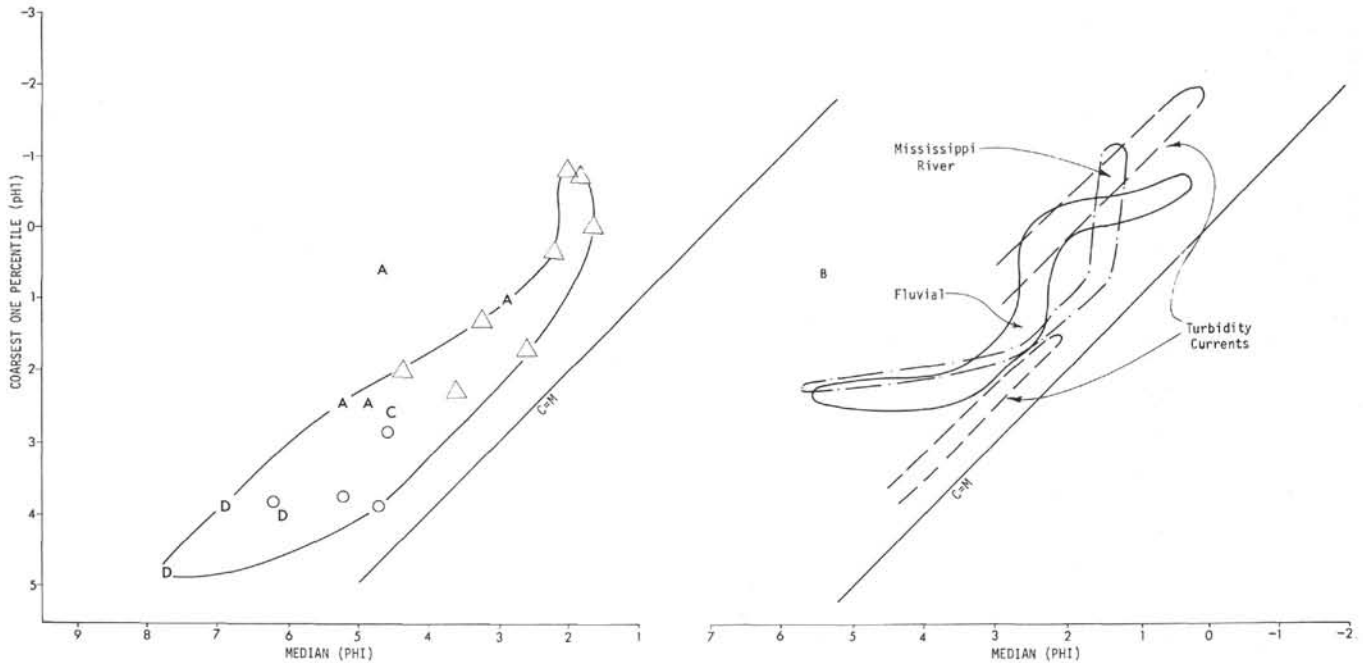


Figure 10. A. C-M Diagram for turbidites. Each point represents one sample with the size of the coarsest one percent plotted against size of the median. The massive sands ( $\Delta$ ) and graded beds (A,C,D,O) include samples from the flysch, Site 241. A,C,D, represent the respective Bouma interval from which the graded bed samples were taken. O specifies graded bed samples unidentified with respect to Bouma interval. Excepting one anomalous analysis (see Figure 5) the data outline an envelope trending parallel to the line C=M, but steepening at the coarser end. Note that the analyses of massive sands overlap the graded beds (A-Bouma intervals).

#### Massive Sands

The probable transport distances of the massive sands should be established before discussing their depositional processes. Massive sands at both Sites 240 and 248 are predominantly Miocene in age. If we assume there have been no large changes in relative topography since this time, we may use the modern bottom configuration as a guide to dispersal patterns. It follows that the probable distance of transport to Site 240 was 750 km, the current minimum distance to the shelf edges of Africa and Madagascar (Figure 11). The granitic basement of the Seychelles Islands can be ruled out as a significant sediment source since it is of small aerial extent and is shielded from Site 240 by extremely rough topography. Moreover, if a density current should thread its way through this rough topography, its path to Site 240 would be more than 750 km. Modern abyssal slopes in the vicinity of Site 240 do not exceed 1:1000. Density current flow to Site 240 apparently moved in a direction normal to the local continent edge (see Figure 11).

Although Site 248 is located adjacent to the prominent Mozambique Ridge (Figure 12), this feature could not have been a mid-late Miocene source of coarse clastic detritus since it was accumulating pelagic sediment at this time (see

B. Compilation of C-M Patterns (after Passega, 1957, 1964). Shown here are C-M patterns for: (1) a generalized fluvial system, (2) turbidity currents (position varies between envelopes shown depending on density), (3) the empirical pattern of Mississippi River sediments. In all cases, segments trending parallel to C=M are considered to be deposits of graded suspensions. The lower horizontal portions of the general fluvial curve and the Mississippi River curve are apparently deposits of the suspended load. The vertical trend of the Mississippi River envelope and the upper horizontal and vertical trend of the generalized fluvial curve are bed load deposits.

Lithology, Site 249). The closest approach of the African shelf edge to Site 248 is 475 km. However, the topographic high of the Mozambique Ridge would have probably prevented density current flow along this most direct path. It is likely that the medium to coarse sands of Site 248 were supplied by density currents flowing down the Mozambique Channel, probably through the Zambezi Submarine Canyon (Figure 12). The minimum distances of transport from the shelf edges of Africa and Madagascar to Site 248 via the Zambezi Canyon system are 1770 and 1420 km, respectively. In the vicinity of Site 248, the slope trending up the Zambezi Canyon is currently less than 1:900. In contrast to Site 240, density current flow to Site 248 was predominantly parallel to the local continental edge.

Massive sandstone beds are a common component of subaerially exposed turbidite sequences (Moore, 1973; Stanley, 1969b; Stauffer, 1967). They are assumed to have been deposited in submarine canyons or submarine distributary channels. Supporting this conclusion, Leg 25 drilling (Sites 243, 244) recovered coarse sand and gravel from the Zambezi Submarine Canyon. The available data do not indicate whether the massive sands of Sites 240 and 248 were deposited in submarine distributary channels or as sheet sands.

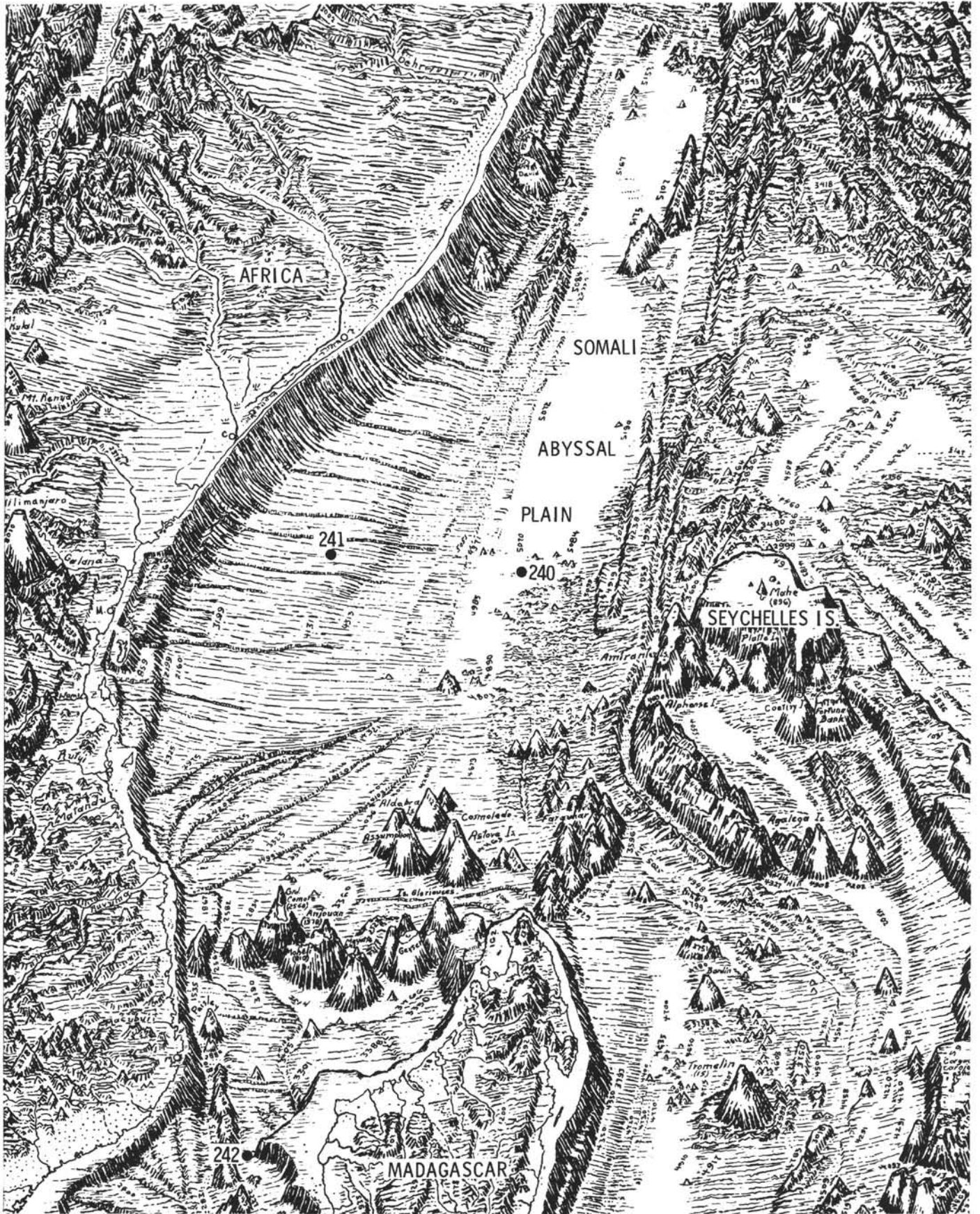


Figure 11. Physiographic setting of Sites 240, 241 and 242. Base map from Heezen and Tharp (1964).



Figure 12. Physiographic setting of Sites 239, 242, 243, 244, 245, 246, 247, 248, 249.

Previous workers have proposed that massive sands (sandstones) are deposits of mass flows, grain flows, and turbulent suspensions. Gravity creep and sand flow (Dill, 1964) are undoubtedly of considerable importance in transporting sand down submarine canyons with steep gradients, but this process is probably not active on the abyssal plain where the massive sands of Site 240 and 248 were deposited. A grainflow mechanism has been used by Stauffer (1967) to explain massive sandstone beds in a turbidite sequence of the Santa Inez Mountains, California. Even with interstitial mud matrix capable of sustaining excess pore pressures, grain flows require slopes of several degrees for sustained transport of sediment (Middleton, 1970). Dzulynski et al. (1959) suggest massive sandstones ("fluxo-turbidites") are transitional between slumping and

turbulent suspension. Based on internal amalgamation and large basal flute casts, I have previously interpreted massive sandstones as proximal turbidity current deposits (Moore, 1973).

The massive sands cored on Leg 25 provide some additional insights into depositional processes of these sediments. Though the cores were too unconsolidated to preserve primary sedimentary structures (if there were any), textural evidence from the detailed grain-size analyses may be used to interpret the depositional processes of these massive sands.

The *C-M* diagram (Figure 10A) presents a particularly useful summary of grain-size data for the massive sands. This plot characterizes each sample by its coarser half and thus is not highly sensitive to the effects of washing (which

may selectively remove the finest fraction). The broad envelope paralleling the line  $C=M$  is typical of turbidity current deposits (Passega, 1957, 1964). The sharp increase in  $C$  relative to  $M$  at the coarser end of the envelope defines a pattern similar to that shown by bed loads of tractive currents (Passega, 1957, 1964). Note that the upturned portion of the massive sand envelope falls between Passega's idealized "complete traction current pattern" and the actual  $C-M$  pattern of the Mississippi River bed load (Figure 10B). The rapid increase in  $C$  is explained (Passega, 1964) by the ability of a current to move much coarser particles in the bed load than it can carry in graded suspension. Therefore, in the initial stages of bed load transport, the coarsest fraction increases rapidly without effecting the median grain size. Finally, note that the  $C-M$  pattern of massive sands is transitional to more proximal portions of the turbidite pattern (A-Bouma intervals). These data suggest that the depositional medium of the massive sands had characteristics of the bed load of traction currents but was transitional to a turbulent suspension. Portions of the massive sands may be the deposits of a traction carpet formed at the base of a turbulent suspension.

Rizzini and Passega (1964) and Passega (1964) present  $C-M$  patterns of massive sandstones ("unda-turbidites", N. Apennines, Italy) which show  $C-M$  patterns broadly similar to the one presented here. They suggest that the massive sandstones were deposited by turbidity currents but reflect the grain-size distribution of the tractive current sediments from which they originated. This interpretation probably would not apply to the massive sands cored on Leg 25 as their transport for many hundred kilometers probably would have thoroughly re-sorted them to reflect their actual depositional process. Admittedly, my interpretation is based on meager data and should be tested by more complete textural studies. It is worthwhile to point out that the analyses defining the upturn in the  $C-M$  envelope were not washed during drilling (note graphic and visual aspects, Figure 8) and must be considered as accurate data.

Regardless of the depositional process, these medium to coarse massive sands have been transported at least 750 km (Site 240), possibly up to 1750 km (Site 248) over slopes as low as 1:1000 to abyssal depths. Thus, the presence of massive sandstone in uplifted turbidite sequences is not necessarily an indication of slope or base of slope environment but simply suggests the presence of a source capable of supplying large quantities of sand. In the western Indian Ocean, this terrane is the crystalline basement of Africa and Madagascar.

#### Laminites

Many geologists generally attribute the deposition of laminites to turbidity currents (e.g., Lombard, 1963; Beall and Fischer, 1969); however, the specific evidence supporting this conclusion is often ambiguous. The sometimes graded, but often ungraded and even reverse graded, laminites cored on Leg 25 further contribute to the confusion.

Deep thermo-haline currents possibly attain velocities capable of transporting the silt-sized material observed in the laminites. The reverse grading and sharp top and

bottom contacts of the laminites at Sites 241 and 248 are consistent with their deposition by contour currents (Bouma and Hollister, 1973). The silt layers of some laminites at Site 241 contain abundant calcium carbonate. Since the flysch sequence containing the laminites was apparently deposited below the prevailing CCD, the laminites, like the associated graded beds, must have accumulated rapidly to prevent complete dissolution on the sea floor. Thus, the laminites containing carbonate silt may have been deposited by extremely distal turbidity currents and covered by mud settling out of the water column.

#### Source Areas

All major turbidite bed types include a predominance of silicate minerals apparently derived from the crystalline basement terranes of Africa and Madagascar. The best evidence of this provenance is the abundance of quartz and potassium feldspar (including microcline). The "granitic" rock fragments suggest the presence of intrusive or gneissic exposures in the source areas, whereas the pink garnets were probably derived from high grade metamorphic rocks. The ubiquitous green hornblende could have originated from either igneous or metamorphic rocks. Rare volcanic glass suggests minor volcanic provenance. A detailed discussion of probable source areas for the turbidite sands is contained in Girdley and White (this volume).

The biogenic detritus of the turbidite beds tags the silicate fraction, revealing its movement through various faunal environments. Shallow-water foraminifera and *Balanus* fragments clearly indicate inner shelf conditions. Movement of the turbidites into the deep ocean is chronicled by their incorporation of various abyssal benthonic microfossils. The greater proportion of biogenic detritus in the graded beds, relative to the massive sands, may indicate derivation of the turbidites from different source reservoirs. However, the apparent similarity of the silicate fraction suggests that size-mass sorting or transport along different paths may account for the variations in biogenic detritus. For example, it is possible that massive sands are channel deposits and the graded beds represent overbank deposits. The graded beds could have incorporated a large proportion of abyssal benthonic microfossils after exceeding the confines of the turbidity current channel. A detained study of sedimentary texture and the paleoecology of the micro-fauna of the turbidite beds might serve to distinguish between these possibilities.

### TERRIGENOUS MUDS

#### Main Sediment Types

Terrigenous muds comprise a significant component of sediments cored on Leg 25. This fine-grained detritus is relatively undiluted in cores from Sites 239, 240, and 241 but is mixed with pelagic and volcanic sediment at Sites 242, 245, 248, and 249. In this report, I have chosen to concentrate on the best defined occurrences of terrigenous muds (Sites 239, 240, and 241). The petrology of fine-grained volcanic sediments (Sites 248, 249, and ash beds at other sites) is treated by Vallier (this volume), whereas Leclaire (this volume) discusses occurrences of true pelagic brown clays.

The lithology, paleontology, and distribution of terrigenous muds is summarized below, primarily from shipboard descriptions. Cores 1-10 (0-158 m, Pleistocene-middle Miocene) from Site 239 contain variable amounts of green and gray silty clay mixed with foram and nanno ooze. In contrast, Cores 11-18 (158-309 m, middle-early Miocene, middle Eocene, early Paleocene) comprise a conspicuous unit of brown clay. Smear slide observations indicate an abundance of silt-size quartz and feldspar, which, coupled with an absence of authigenic minerals, suggest predominantly terrigenous origin for the brown clay. At Site 240, green clay and yellow-brown and green silty clay are interbedded with biogenic ooze and massive sand from 0 to 186 meters (Quaternary-late Miocene, early Eocene; Cores 1-5, Hole 240; Cores 1 and 2, Hole 240A). The terrigenous muds of Site 240 do not comprise a major stratigraphic unit but are dispersed through the cored section. The upper 16 cores (0-464 m, Holocene-late Oligocene) from Site 241 include a sequence of dark greenish-gray silty clays. Relatively pure silty clay occurs in Cores 13-16 (322-464 m, middle Miocene-late Oligocene); whereas, the silty clay component is diluted by various proportions of biogenic detritus in Cores 1-12 (0-303 m, Holocene-middle Miocene). Cores 17-29 (483-1174 m, middle Eocene-Turonian), Site 241 comprise the thickest terrigenous sequence penetrated during Leg 25. In this section, brown clay comprises most of Cores 17-21 (483-587 m, middle Eocene-Paleocene), green and brown clay with up to 15 percent nannofossils make up Cores 22-24 (626-758 m, Campanian), and carbonate-free green and brown clay is included in Cores 25-29 (835-1174 m, Turonian-early Senonian).

Although I will not discuss the petrology of the pelagic brown muds (Site 245), the volcanic derived muds (Site 248), or the clayey nanno-chalk (Site 242), their positions in time and space are relevant to the overall interpretation of hemipelagic sedimentation. The green mud and laminites of Site 248 comprise Cores 10-13 (312-407 m, Eocene). At Site 245, pelagic brown clays occur from 0-63 meters (Cores 1 and 2 of Holes 245 and 245A, Quaternary?-middle Miocene [?], late Eocene). By comparison of carbon-carbonate and insoluble residue analyses, it is clear that clay content increases with age in the ooze and chalk of Site 242. At this location, Cores 5-19 (237-676 m, late Miocene-early Eocene) show a conspicuously increased clay content locally comprising more than 50 percent of the rock (see lithology, Site 242).

## Composition

### General Observations

The following petrologic discussion is based primarily on smear slide and X-ray data. Smear slides are used to determine percentages of quartz and feldspar relative to clay minerals. X-ray data are used to estimate proportions of minerals of similar crystallinity (e.g., quartz-plagioclase-potassium feldspar ratios, and ratios of various clay minerals). Major trends in X-ray mineralogy are covered in the next section.

Due to time limitations, my analysis of the terrigenous muds relies on the smear slide and X-ray data from the

relatively pure, noncalcareous sections. Hopefully, this information accurately represents the fine-grained terrigenous sedimentary end-member which is mixed in all proportions with true pelagic deposits.

The brown mud of Cores 11-18 comprise the major terrigenous lithology of Site 239. They are composed of 70-90 percent clay with 10-30 percent quartz, feldspar, and heavy minerals. X-ray data indicate that potassium feldspar is about equal in abundance to quartz plus plagioclase. The clay mineralogy of the brown mud is highly variable, but most samples show a predominance of montmorillonite. Detrital chlorite occurs in silt-size particles in most smear slides. A large (>silt-size) sheet silicate of low birefringence is present in several smear slides. Since the X-ray data show an abundance of illite-mica in these samples, and since individual particles of montmorillonite and palygorskite are generally very fine, the unknown mineral may be mica, possibly of detrital origin. Its low birefringence may be due to preferred orientation parallel to cleavage. Manganese nodules occur in Core 15, Sections 2 and 3. Pyrite and iron oxides comprise minor amounts of several smear slide samples. Hornblende, zircon, and epidote occur in trace abundances.

The green-gray mud of Site 240 includes 70-95 percent clay minerals with 5-30 percent quartz, feldspar, and heavy minerals. Quartz, potassium feldspar, and plagioclase occur in approximately equal amounts, whereas montmorillonite is the predominant clay mineral. Opaque minerals (largely pyrite) occur in amounts up to 3 percent; chlorite comprises up to 1 percent of some smear slides; rutile and palagonite are present in trace amounts.

The mud and mudstone (Cores 19-29) of Site 241 may be conveniently divided into green and brown end-members. Since no significant differences in lithology were noted between the mud and their consolidated equivalents (mudstone), they are all referred to as mud. Quartz, feldspar, and heavy minerals comprise 5-55 percent (avg. 20%) of the green mud, whereas, clay content ranges from 45 to 95 percent. Potassium feldspar is usually more abundant than plagioclase, but quartz is highly variable. Chlorite and montmorillonite are about equal in abundance to the sum of mica, kaolinite, and palygorskite. A silt-size sheet silicate of low birefringence is present in several smear slides. Similar to Site 239, the X-ray data suggest this mineral is detrital mica. Chlorite occurs locally in amounts of up to 3 percent. Trace abundances of pyrite, hornblende, biotite, and volcanic glass are present in the green mud.

Many of the same minerals occur in the brown mud as in the green mud. The brown mud contains 80 to 93 percent clay and 7 to 20 percent quartz, feldspar, and heavy minerals. Potassium feldspar is more abundant than plagioclase, and quartz is highly variable. Of the clay fraction, montmorillonite is predominant, occurring with lesser amounts of palygorskite, mica, and kaolinite. Iron oxides (amorphous oxides-goethite-hematite) are conspicuously present in the brown mud, locally reaching concentrations of 5 percent. The brown mud also includes traces of chlorite, volcanic glass, and zircon. Thus, the brown mud from Site 241, as compared to the green mud, contain less quartz and feldspar and more clay, but the proportions of minerals within each of these groups is

similar. The brown mud is more highly oxidized than the green muds (iron oxides vs. iron sulphides, respectively).

In summary, the abundant potassium feldspar, with minor amounts of chlorite, hornblende, zircon, and rutile, confirm the predominantly continental origin for both green and brown muds of Sites 239, 240, and 241. The oxidation of iron minerals and smaller proportions of quartz and feldspar in the brown mud suggest slower sedimentation rates relative to the green mud.

#### Trends in X-ray Mineralogy

In addition to specifying the composition of individual units, X-ray data provides a measure of mineralogical trends in time and space. Although the absolute accuracy of semiquantitative X-ray work is debatable, the analyses utilized here are probably internally consistent. The following analysis is concentrated on the relatively pure terrigenous sediments from Sites 239 (Cores 11-18), 240 (Hole 240, Cores 1, 3, 5; Hole 240A, Core 1), and 241 (Cores 12-29). Comparisons are made to X-ray data from Sites 245 and 248 (Cores 10-13).

An obvious plot of X-ray data involves comparison of abundances of quartz and feldspar to clay minerals. Specifically, the ternary diagram, quartz + feldspar-montmorillonite + other clays, broadly separates the green and brown mud (Figure 13). The relative enrichment of the green mud in quartz and feldspar is best demonstrated by the data from Site 241 (Figure 13). The overlap in composition of the green and brown mud emphasizes the continuous gradation between these two lithologies.

A ternary plot of kaolinite + mica - montmorillonite + chlorite - palygorskite demonstrates a strong identity for the  $<2\mu$  fraction (decalcified) from Sites 240, 241, and 248 (analyses from each Site are outlined on Figure 14). The data for Site 239 are less well grouped, encompassing the major clusters for Holes 240 and 241. Montmorillonite is in fact the major component of the montmorillonite + chlorite end member of all analyses since nowhere does chlorite exceed 4 percent of the  $<2\mu$  fraction. Kaolinite + mica (including illite) occur in various proportions and are grouped together due to their compositional similarity.

The ternary plot of clay minerals (Figure 14) shows that some samples are anomalously enriched in palygorskite. This trend has been further investigated by a scatter plot of montmorillonite vs. palygorskite (Figure 15). The plot demonstrates a broad inverse correlation between the two minerals for green, brown, and turbidite mud. The correlation is better defined by a single lithology, the green mud (Figure 15). The turbidite mud also shows the same broad inverse correlation for palygorskite content in the 4-35 percent range. These relationships must be interpreted with care due to the inherent difficulties in ratio correlation of a closed array (Chayes, 1971).

The ternary plot of quartz + cristobalite + tridimite - potassium feldspar - plagioclase (Figure 16) demonstrates clustering of analyses for Sites 239, 240, and 248. The silica enrichment of analyses from Site 248 is consistent with the probable volcanic origin of these sediments. The variations in analyses from Site 241 may be due to the extended time span represented by these data.

The various reconnaissance plots presented above clearly show that terrigenous muds of Sites 239, 240, 241, and 248 can be characterized by X-ray mineralogy. This analysis could be extended to the hemipelagic sediments but would require normalization of their bulk X-ray data to a calcite free basis. Time-stratigraphic variation possibly could be defined by plotting variations in X-ray mineralogy against age. The inverse relationship between palygorskite and montmorillonite will be further discussed under diagenesis.

#### Texture and Sedimentary Structures

This discussion of texture relies largely on grain-size analyses by the DSDP Shore Laboratory since the shipboard visual estimates, though more numerous, are somewhat less accurate. The terrigenous mud of Sites 239, 240, and 241 (carbonate free) include 70-93 percent clay-size particles and 7-30 percent silt; they are predominantly clays. The hemipelagic mud (which include pelagic microfossils) are silty-clay with 28-46 percent silt. Silt-sized microfossils apparently cause the coarsening of the hemipelagic sediments relative to their pure terrigenous component. Petrographic data suggest that the brown mud is finer grained than the green mud; however, grain-size analyses were too few in number to confirm this observation.

Burrows and fissility are the only significant sedimentary structures observed in the terrigenous mud. Burrows occur in varying intensity in some terrigenous sections. The mudstones cored at Site 241 are locally moderately fissil.

#### Diagenesis

The following section concentrates mostly on chemical diagenesis; however, some information is included on the effects of downhole consolidation. At all sites, the muds showed a gradual transition from soupy sediments near the mudline to various states of consolidation depending on depth of penetration. Cores from Site 241 are consolidated to mudstone beginning at 530 meters (Paleocene). The lithification of ooze to chalk seems to occur at shallower depths than the mud-mudstone transition, presumably due to early recrystallization of calcium carbonate.

The effects of chemical diagenesis include formation of iron oxides and iron sulfides, and a possible diagenetic relationship between montmorillonite and palygorskite. Pyrite is ubiquitous throughout the green mud (see turbidite diagenesis for probable explanation) but less frequently observed in the brown mud. Pyrite visible in smear slides was not always detected by the bulk X-ray analyses. Amorphous iron oxides, goethite, and hematite account for the coloration of the brown mud. It is reasonable to expect a transition from amorphous iron to goethite to hematite by an aging process similar to that proposed for the development of hematite cement in red beds (van Houten, 1968). The X-ray data from Site 241 support this idea with goethite occurring at 531-585 meters, stratigraphically above hematite at 1170 meters. However, simple goethite-hematite aging doesn't seem to occur in the volcanic sediments of Site 249 since hematite occurs stratigraphically above goethite.

The apparent inverse relationship between palygorskite and montmorillonite implies, but does not prove, a genetic

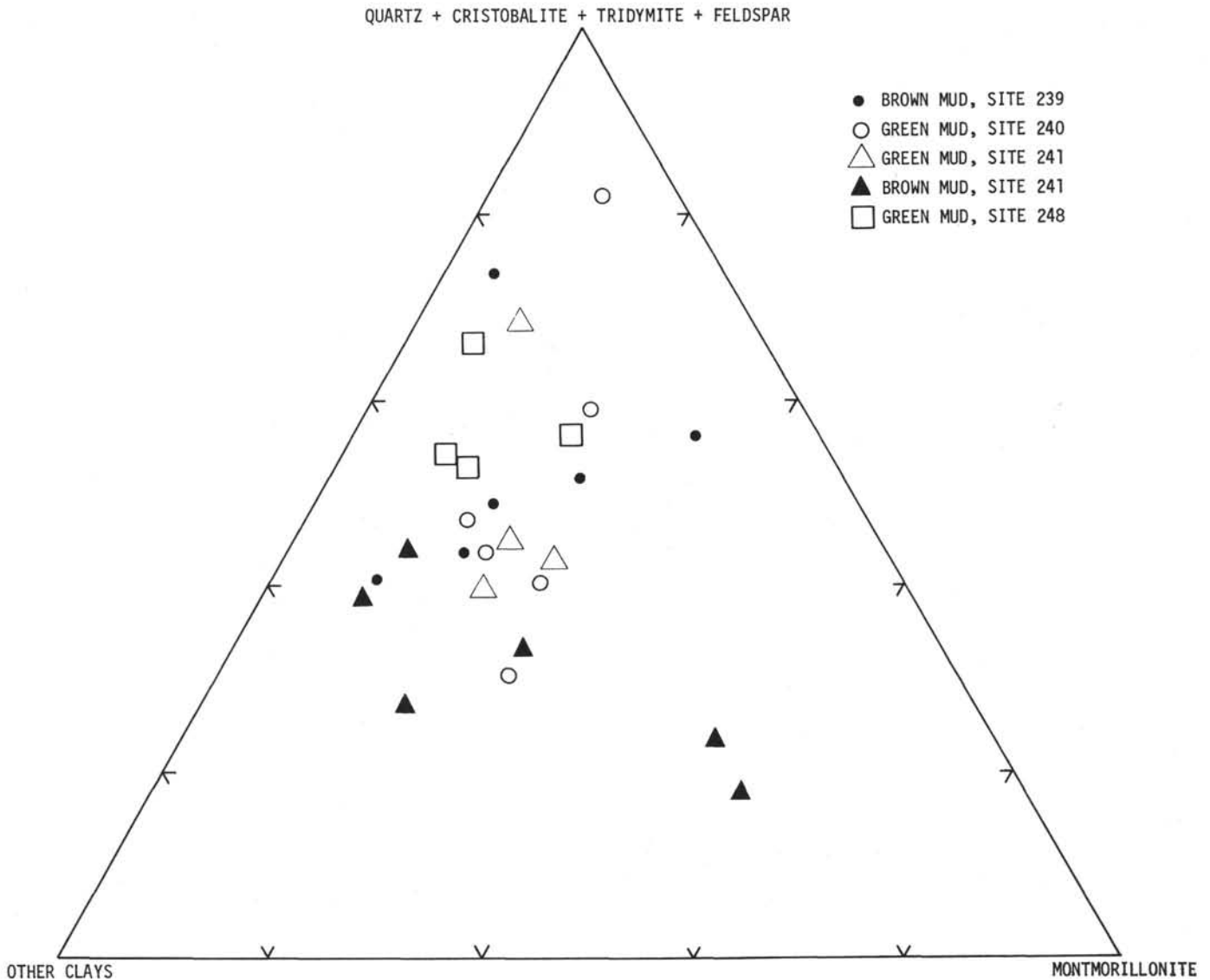


Figure 13. Ternary plot of bulk X-ray mineralogy of terrigenous muds (data from Matti et al., this volume). Note that on the average the brown muds (solid symbols) have greater proportions of clay minerals and lesser amounts of silica and feldspar relative to the green muds.

connection between these two minerals. Within one lithology, the inverse abundances could be generated by alteration from each other, or from a common parent. Bonatti and Joensuu (1968) have proposed that palygorskite plus clinoptilolite alters from montmorillonite; however, palygorskite-bearing terrigenous muds from Leg 25 rarely contain clinoptilolite. Peterson et al. (1970) note an association of palygorskite and volcanic ash, inferring the alteration of the former from the latter. The concentration of both volcanic detritus and palygorskite in the muds from Site 248 is consistent with this view. Bowles et al. (1971) attribute the formation of palygorskite to chemical precipitation. The Leg 25 muds show no direct evidence supporting this origin. I favor the development of palygorskite by alteration of volcanic material, though admittedly the existing data provides no conclusive solution to the problem. Possibly, a detailed mineralogical and textural investigation of the palygorskite-bearing muds would yield an answer.

#### Depositional Processes and Source Areas

The homogenous terrigenous muds provide no positive internal evidence of a depositional medium as do graded beds. The lack of variation within the muds favors accumulation by steady state processes such as grain by grain settling and nephloid transport. The agent responsible for transporting these muds must be capable of moving predominantly clay-sized sediment (7%-30% silt) at least 750 km (minimum distance separating Site 240 from shelf edge, Figure 11). The terrigenous muds of Sites 239, 240, and 241 could have entered the sea through the small rivers along the eastern borders of the Somali and Mascarene basins or by eolian transport from Africa.

Months, or even years, may be required for the slow descent of clay or fine silt particles through the water column. Slow settling of very fine sediment combined with favorable current movement can probably account for hundreds of kilometers of transport before deposition

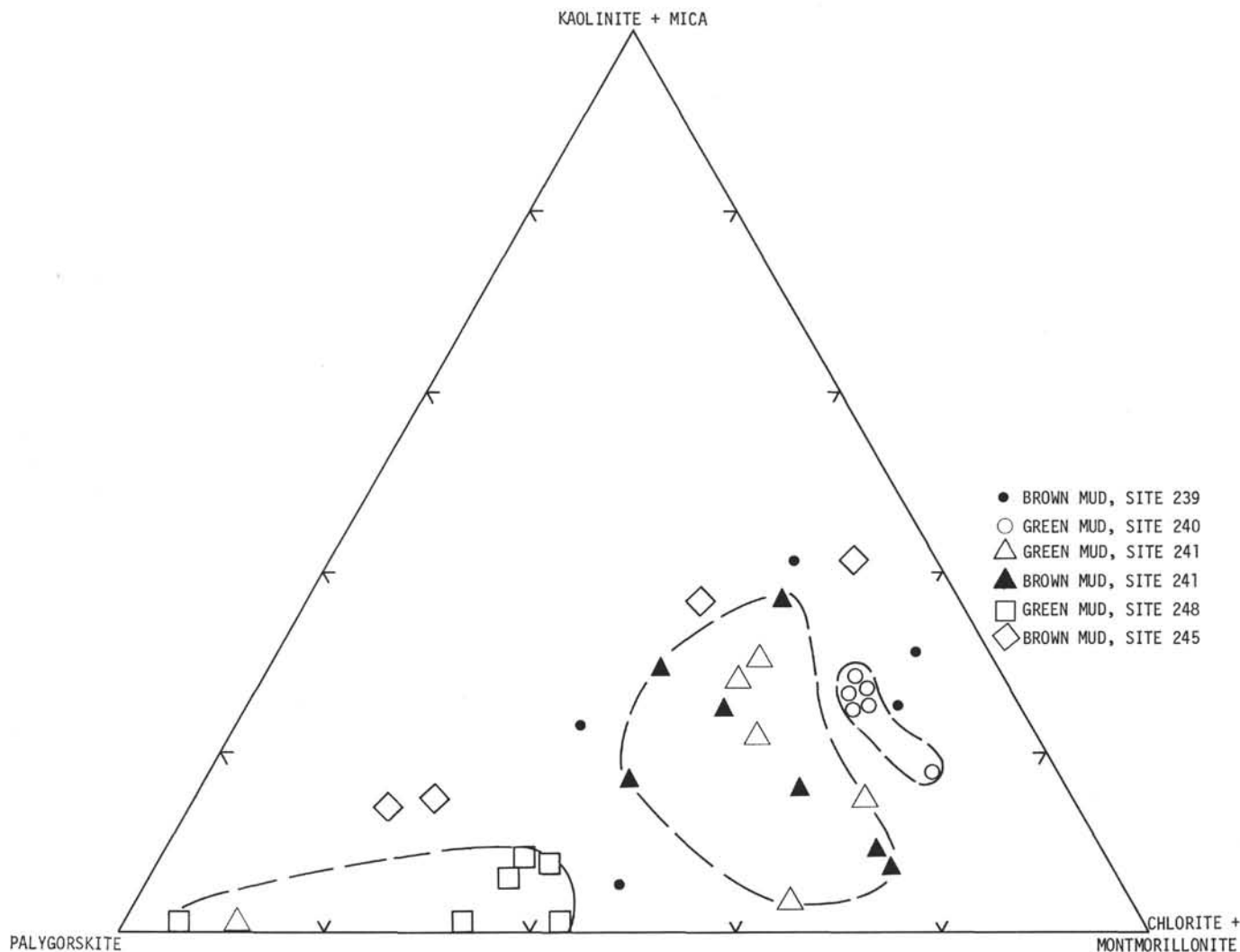


Figure 14. Ternary plot of X-ray mineralogy of clays ( $<2\mu$  fraction-decalcified, data from Matti, et al., this volume).

(Jacobs and Ewing, 1969). The proximity of Sites 239 and 241 to continental land masses suggests much of their fine-grained terrigenous component may have simply settled out of the water column.

To my knowledge, no specific model of deep current circulation has been proposed for the western margin of the Indian Ocean. Present, the Southwest Indian Ridge forms a relatively continuous topographic barrier between the Antarctic deep water and abyssal basins adjacent to East Africa. Preceding the late Tertiary development of the Southwest Indian Ridge, Antarctic deep water may have flowed northward along the East African continental margin. This current would have been intensified due to the earth's rotation and may have been strong enough to entrain fine-grained sediment. A western boundary current off eastern North America, possibly similar to the current postulated above, includes suspended sediment which defines a nephloid layer (Eittrheim et al. 1969).

If nephloid layer transport occurred off East Africa during the Cretaceous and Tertiary, sediment could have been injected into this suspension by turbidity current plumes, grain by grain settling, and activity of burrowing sea floor organisms. Cores for Sites 239, 240, 241, and 248

include some indications of burrowing and ample evidence of turbidity current deposition during terrigenous mud sedimentation. Moreover, the coarser silt particles of the terrigenous muds from Sites 239, 240, and 241 contain many of the same minerals as the associated turbidites.

In summary, a combination of grain by grain settling and nephloid transport (with input from turbidite plumes) can account for the distribution of terrigenous muds cored on Leg 25. The lack of facies equivalency between Sites 239, 240, and 241 suggests localized sources and a lack of large scale interbasinal sediment transport. The abundance of potassium feldspar and heavy minerals reflect derivation from the continental basement of Africa and Madagascar.

## CONCLUDING REMARKS

### Suggestions for Further Work

This preliminary study of the turbidites and terrigenous muds cored on Leg 25 has touched upon many exciting topical problems. Some of the most interesting problems are: (1) the depositional mechanisms of the massive sands, (2) the paragenesis of palygorskite, and (3) the diagenesis of the flysch sandstones. The massive sands are definitely

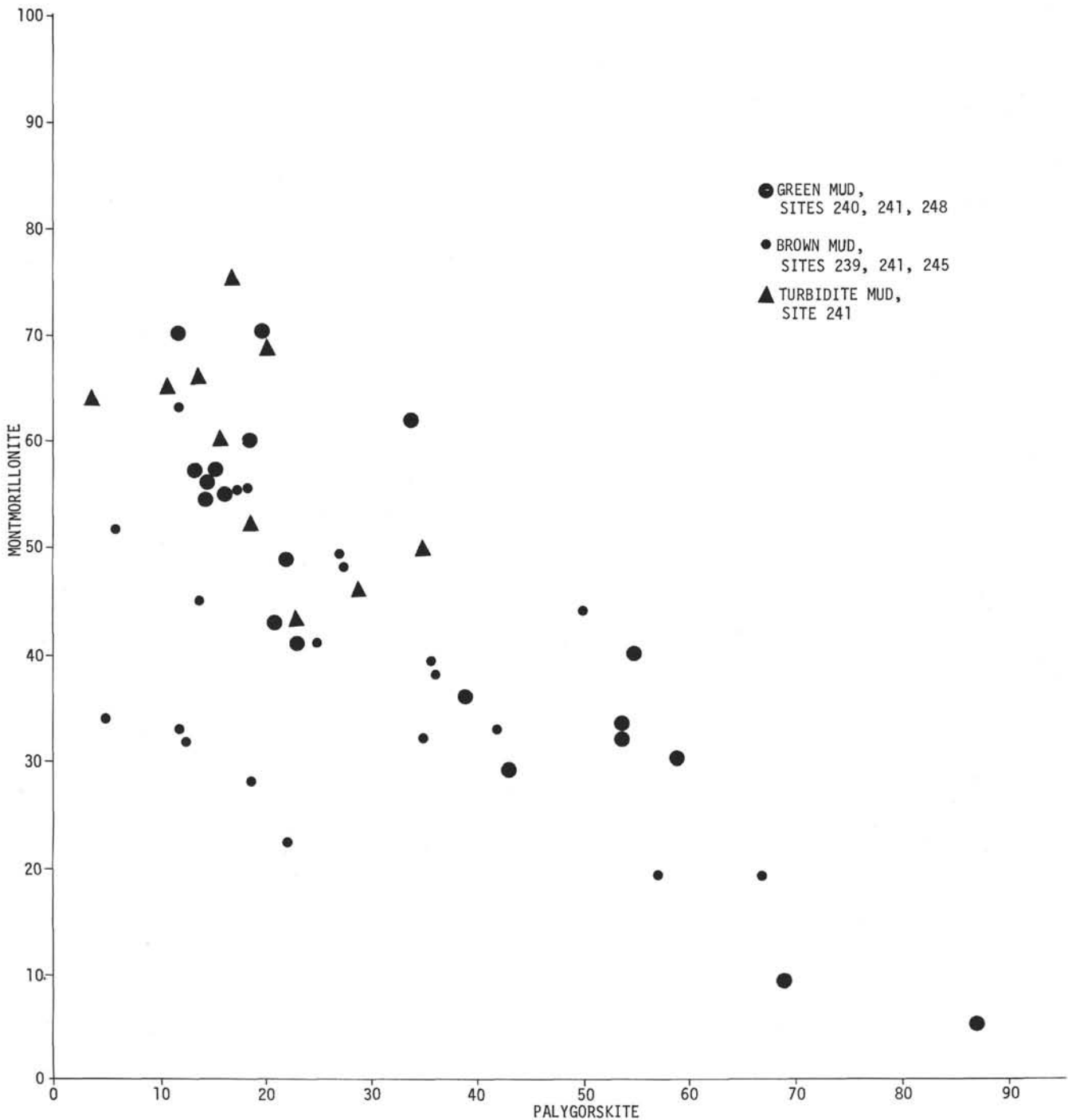


Figure 15. Scatter plot of montmorillonite vs. palygorskite (*X-ray mineralogy of 2 fraction-decalcified, data from Matti, et al., this volume*).

worth further textural study (both mechanical and microscopic) to further establish the mechanism which transported these deposits over abyssal slopes. Both the textural relations and mineralogy of palygorskite and associated clays and volcanic materials should be studied in detail to determine the origin of this unusual mineral. The flysch sandstones deserve further textural and mineralogical investigations to determine if, in fact, organic matter locally prevented their neomorphic recrystallization. Moreover, it would be of interest to measure the volume of silica

removed, in solution, from these rocks and estimate (using modified interstitial water composition) the pore volumes of water necessary to complete this process.

#### Aspects of Geologic History

The variability of facies between Leg 25 sites precludes a detailed discussion of geologic history based solely on terrigenous deposits; however, a few general comments are warranted. Although the major terrigenous deposits at Sites

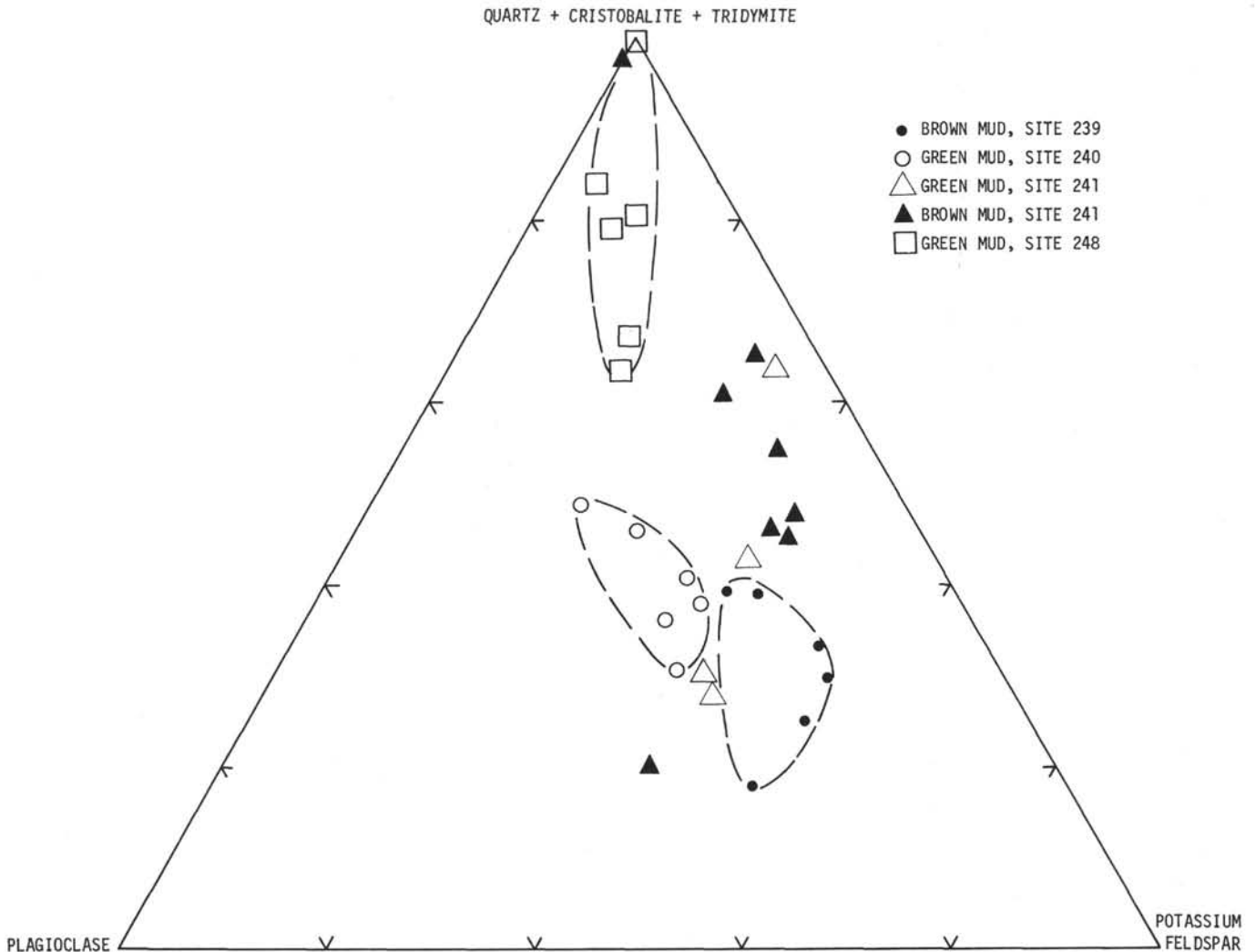


Figure 16. Ternary plot of X-ray determinations of silica minerals and feldspars (bulk fraction, data from Matti *et al.*, this volume). Note dispersion of points from Site 241 relative to those of Sites 239, 240, and 248.

239, 240, and 241 were not specifically correlative, all holes show a greater proportion of biogenic detritus in the Neogene relative to the Paleogene. This variation could be caused by an increase in productivity or a decrease in terrigenous supply. Site 242 provides a test for this proposition since it is/was located above the CCD and has accumulated only pelagic and hemipelagic sediment during the Tertiary. Relative to the Paleogene, the Neogene of Site 242 shows an increase in sedimentation rate (Figure 17) but a relative decrease in proportion of terrigenous sediment (see lithology of Site 242). Thus, these data indicate an increased accumulation of pelagic organisms during the Neogene, which was probably related to increased productivity since depths of deposition at Site 242 were shallow, 2-3 km.

The massive sands cored on Leg 25 were predominantly middle and upper Miocene though some lower Eocene massive sands were cored at Site 240. The Miocene massive sands may indicate orogenic activity of the adjacent continents and partially correlate with an increased Miocene sedimentation rate along coastal Tanzania (Kent *et al.*, 1971). Moreover, the lower Eocene massive sands correlate

well in time and space with accelerated early and middle Eocene sedimentation rates in coastal Tanzania (Kent *et al.*, 1971). At Site 241, the lack of deposits equivalent to the Eocene and Miocene sands of Site 240 apparently indicates efficient bypassing of the continental rise by coarse detritus, probably via well-defined submarine channels.

#### Relevance to Interpretation of Geosynclinal Sequences

Sedimentary sequences of modern continental margins may serve as models for interpretation of ancient geosynclinal deposits. The deep-sea terrigenous sediments cored on Leg 25 are clearly deposits of a complexly rifted continental margin. Later in their history, these sediments could become highly deformed and detached from their basement terrain during an orogenic episode (e.g., a continental collision). Therefore, it behooves us to consider how these sediments represent their depositional and tectonic environment and how we might recognize a similar sequence in a complexly deformed mountain belt. I emphasize the deposits of turbidity currents since they are often key elements in paleogeographic reconstructions. In subaerially exposed sequences, turbidites provide clues to

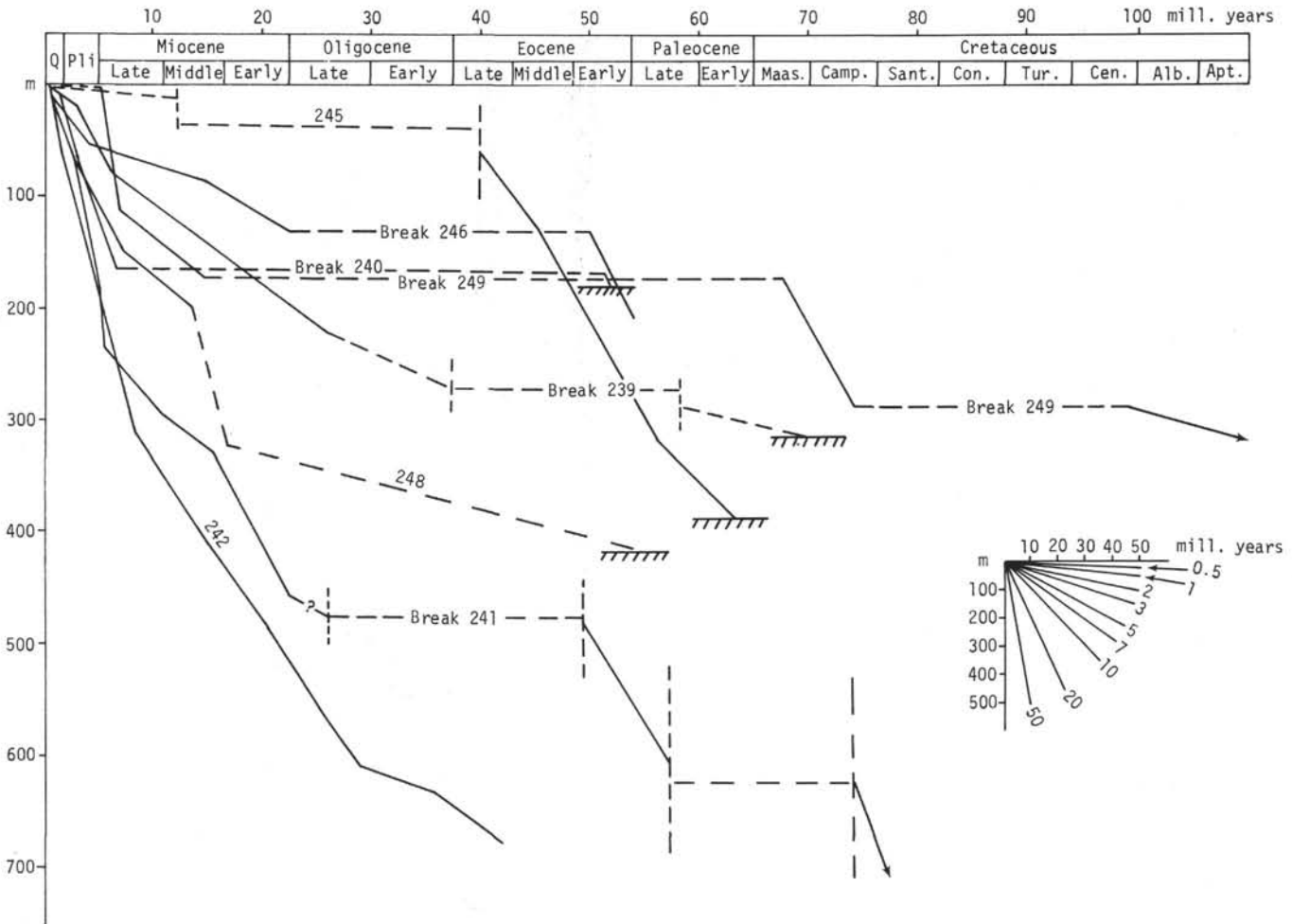


Figure 17. Sedimentation rates, Sites 239, 241, 242, 245, 246, 248, and 249.

both source terranes and basin geometry through respective study of their sandstone petrography and sedimentary structures.

Idealized models can serve to clarify our thinking even though they rarely occur in nature. At a rifted continental margin, turbidites and terrigenous deep-sea muds would accumulate on the continental slope and rise and adjacent abyssal plain. Sedimentary facies in these environments would probably be quite complex; however, the provenance and directions of depositional current flow should be predictable. A rifted continental margin has a high probability of exposing a crystalline basement terrane due to the divisive processes by which the margin forms. Thus, sediments accumulating subsequent to rifting should reflect the basement terrane plus any volcanic material extruded during continental separation. At a rifted continental margin, density currents would move normal to the continental slope and flow unrestrained to the abyssal plain.

The provenance of the terrigenous deep-sea sediments cored on Leg 25 clearly reflects the ideal, showing the overwhelming influence of Africa's crystalline basement but with minor volcanic input. Probable directions of turbidity current flow into the Somali Basin are normal to the

continental margin as expected. However, the probable flow of turbidity currents parallel to the continental margin into the Mozambique Basin does not follow the model of a simply rifted margin. This longitudinal flow apparently is due to the restraining effect of the Madagascar-Madagascar Ridge microcontinental fragment. The flysch sequence at Site 241, with its graded beds and slump folds, accurately represents some generalized conceptions of base of slope deposits (Stanley, 1969a). However, the thick massive sands cored on the abyssal plain at Site 240 are much coarser than those normally expected in the basinal environment (Stanley, 1969a). Certainly these deposits are not proximal slope and base of slope channel deposits, for which they could be mistaken in the stratigraphic record.

#### REFERENCES

- Bathurst, R. G. C., 1971. Carbonate sediments and their diagenesis: New York (Elsevier Publ. Co.), 620 p.  
 Beall, A. O. and Fischer, A. G., 1969. Sedimentology. In Ewing, M., Worzel, J. L., et al., Initial Reports of the Deep Sea Drilling Project, Volume I: Washington (U. S. Government Printing Office), p. 521.  
 Berner, R. A., 1971. Principles of chemical sedimentology: New York (McGraw-Hill), 240 p.

- Bonatti, Enrico and Joensuu, Oliva, 1968. Palygorskite from Atlantic deep sea sediments: *Am. Min.*, v. 53, p. 975-983.
- Bouma, A. H. and Hollister, C. D., 1973. Deep ocean basin sedimentation. *In* Middleton, G. V. (Ed.) *Turbidites and Deep Sea Sedimentation: Soc. Econ. Paleont. Min. (short course)*, p. 79-118.
- Bowles, F. A., Angino, E. A., Hosterman, J. W., and Galle, O. K., 1971. Precipitation of deep-sea palygorskite and sepiolite: *Earth Planet. Sci. Lett.*, v. 11, p. 324-332.
- Chayes, Felix, 1971. Ratio correlation: Chicago (Univ. Chicago Press), 99 p.
- Cummins, W. A., 1962. The greywacke problem: *Liverpool Geol. J.*, v. 3, p. 51-72.
- Dill, R. F., 1964. Sedimentation and erosion in Scripps Submarine Canyon head. *In* Miller, R. L., (Ed.), *Papers in Marine Geology (Shepard Commemorative Volume)*: New York (MacMillan), p. 23-41.
- Dzulynski, S., Ksiazkiewicz, M., and Kuenen, Ph. H., 1959. Turbidites in flysch of the Polish Carpathian Mountains: *Geol. Soc. Am. Bull.*, v. 70, p. 1089-1118.
- Dzulynski, S. and Walton, E. K., 1965. Sedimentary features of flysch and greywackes: developments in sedimentology, 7: Amsterdam (Elsevier Publ. Co.), 274 p.
- Eittreim, S., Ewing, M., and Thorndike, E. M., 1969. Suspended matter along the continental margin of North American Basin: *Deep-Sea Res.*, v. 16, p. 613.
- Heezen, B. C., and Tharp, Marie, 1964. Physiographic diagram of the Indian Ocean: Boulder, Colorado (Geol. Soc. Am.).
- Jacobs, M. B. and Ewing, M., 1969. Mineral source and transport in waters of the Gulf of Mexico and Caribbean Sea: *Science*, v. 163, p. 805.
- Kent, P. E., Hunt, J. A., and Johnstone, M. A., 1971. The geology and geophysics of coastal Tanzania: *Nat. Environment. Res. Council, Inst. Geol. Sci., London, Geophys. Paper no. 6*, 101 p.
- Kuenen, Ph. H., 1964. Deep-sea sands and ancient turbidites. *In* Bouma, A. H. and Brouwer, A. (Eds.), *Turbidites (developments in sedimentology)*: Amsterdam (Elsevier), p. 3-33.
- Lombard, A., 1963. Laminites: a structure of flysch-type sediments: *J. Sediments Petrol.*, v. 33, p. 14.
- Middleton, G. U., 1970. Experimental studies related to problems of flysch sedimentation. *In* Flysch sedimentology) in North America: *Geol. Assoc. Canada Spec. Paper no. 7*, p. 253-272.
- Moore, J. C., 1973. Cretaceous continental margin sedimentation, southwestern Alaska: *Geol. Soc. Am. Bull.*, v. 41, p. 1952-1984.
- Passega, Renato, 1957. Texture as a characteristic of clastic deposition: *Am. Assoc. Petrol. Geol. Bull.*, v. 41, p. 1952-1984.
- \_\_\_\_\_, 1964. Grain size representation by CM patterns as a geologic tool: *J. Sediment. Petrol.*, v. 34, p. 830-847.
- Peterson, M. N. A., Edgar, N. T., Cita, M., Gartner, S. Jr., Goll, R., Nigrini, C., and von der Borch, C., 1970. Initial Reports of the Deep Sea Drilling Project. Volume II: Washington (U. S. Government Printing Office), 501 p.
- Rizzini, A. and Passega, R., 1964. Evolution de la Sedimentation et Orogenese, Vallee du Santerno (Apennin Septemtrional), *In* Bouma, A. H. and Brouwer, A. (Eds.), *Developments in Sedimentology: Amsterdam (Elsevier)*, v. 3, p. 65-74.
- Scholle, P. A., 1971. Sedimentology of fine-grained deep-water carbonate turbidites, Monte Antola flysch (Upper Cretaceous), northern Apennines, Italy: *Geol. Soc. Am. Bull.*, v. 82, p. 629-658.
- Stanley, D. J., 1969a. Sedimentation in slope and base-of-slope environments. *In* The new concepts of continental margin sedimentation: *Am. Geol. Inst. (short course lecture notes)* p. DJS-8-1-DJS-8-25.
- \_\_\_\_\_, 1969b. Submarine channel deposits and their fossil analogs ('fluxoturbidites'). *In* The new concepts of continental margin sedimentation: *Am. Geol. Inst. (short course lecture notes)*, p. DJS-9-1-DJS-9-17.
- Stauffer, P. H., 1967. Grain-flow deposits and their implications, Santa Inez Mountains, California: *J. Sediment. Petrol.*, v. 37, p. 487-508.
- van Houten, F. B., 1968. Iron oxides in red beds: *Geol. Soc. Am. Bull.*, v. 79, p. 399-416.
- Walker, R. G., 1965. The origin and significance of internal sedimentary structures of turbidites: *Yorkshire Geol. Soc. Proc.*, v. 35, p. 1-32.



PLATE 1  
Graded Beds

- Figure 1 241-11-3, 63-79 cm. Typical graded bed, base at 78 cm, top at approximately 65 cm. Note subtle cross bedding (75-76 cm) inclined to left.
- Figure 2 241-11-2, 112-124 cm. Thin graded bed, top poorly defined at 113 cm.
- Figure 3 241-11-4, 22-43 cm. Graded bed, basal layer composed predominantly of forminifera, top poorly defined at about 23 cm.
- Figure 4 340-1-3, 2-20 cm. Graded bed, base at 18 cm, top 5 cm. Note apparent base of another graded bed at 5 cm.

PLATE 1

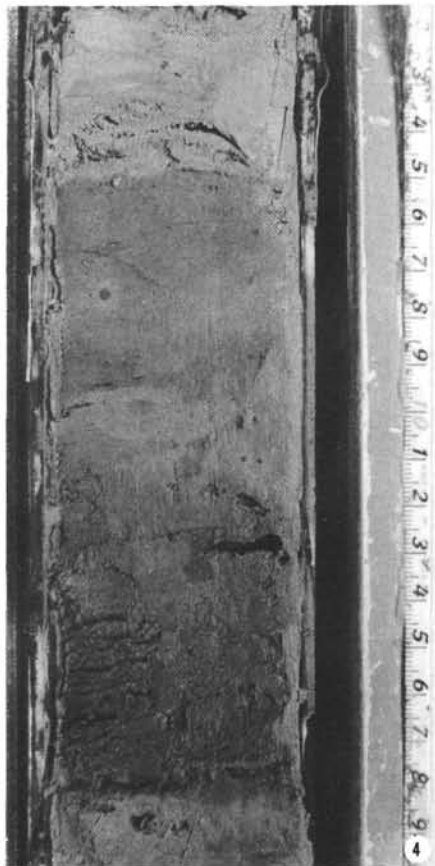
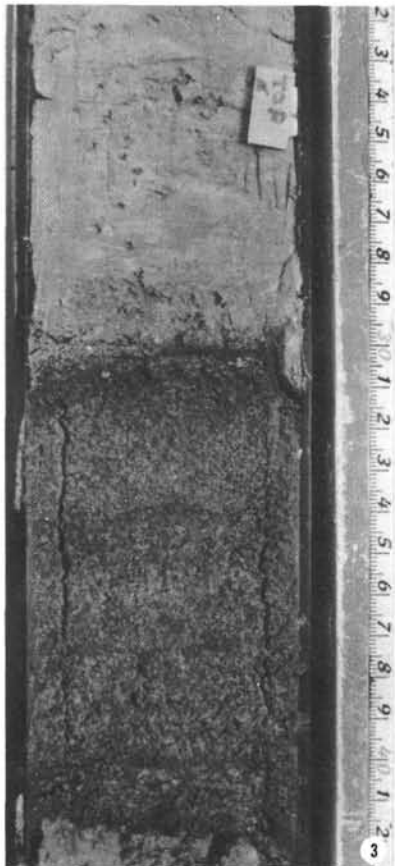
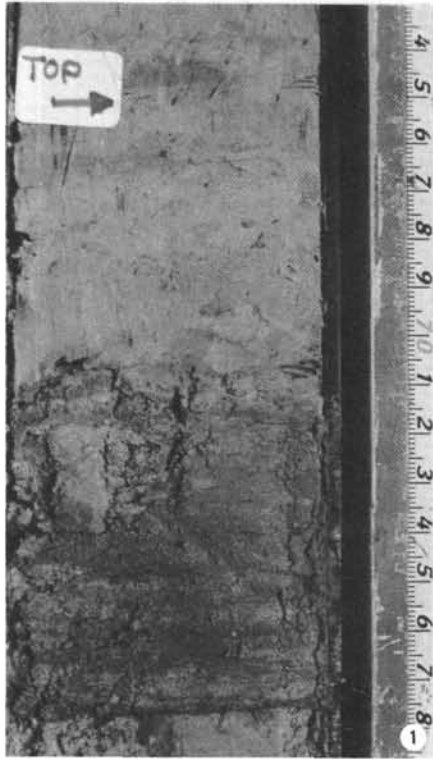


PLATE 2

Massive Sand Bed, 248-8-1, 17-140 cm.

Typical core section of massive sand, note interlayering of sand and mud from 106 to 140 cm.

PLATE 2

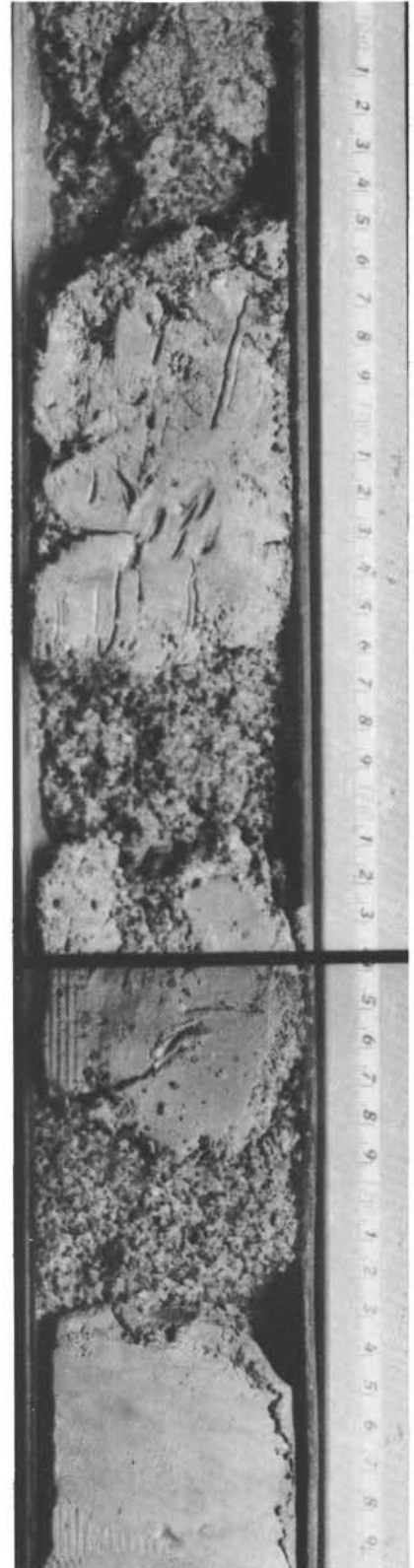
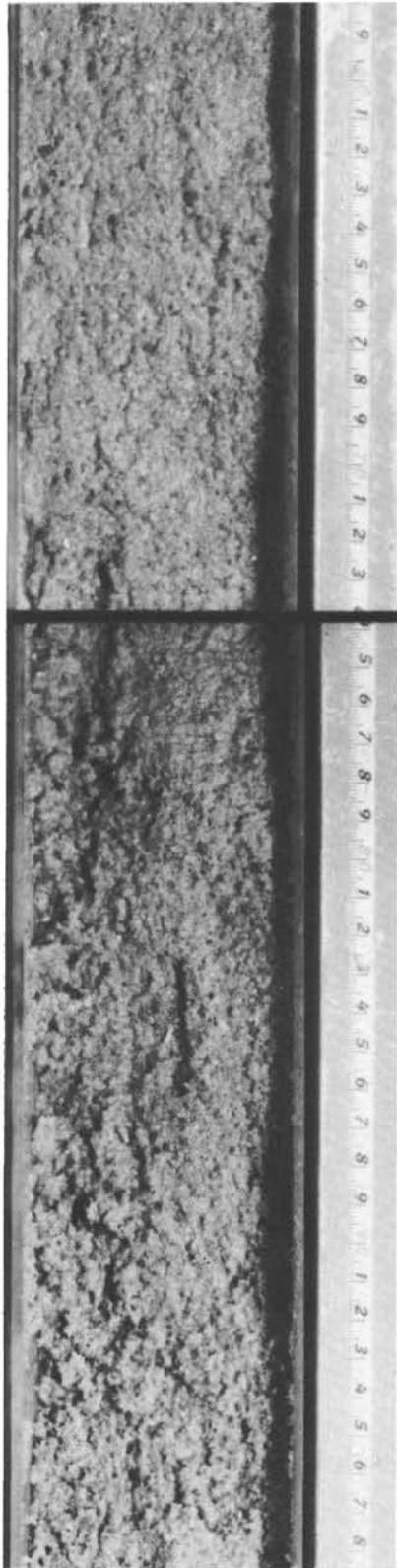
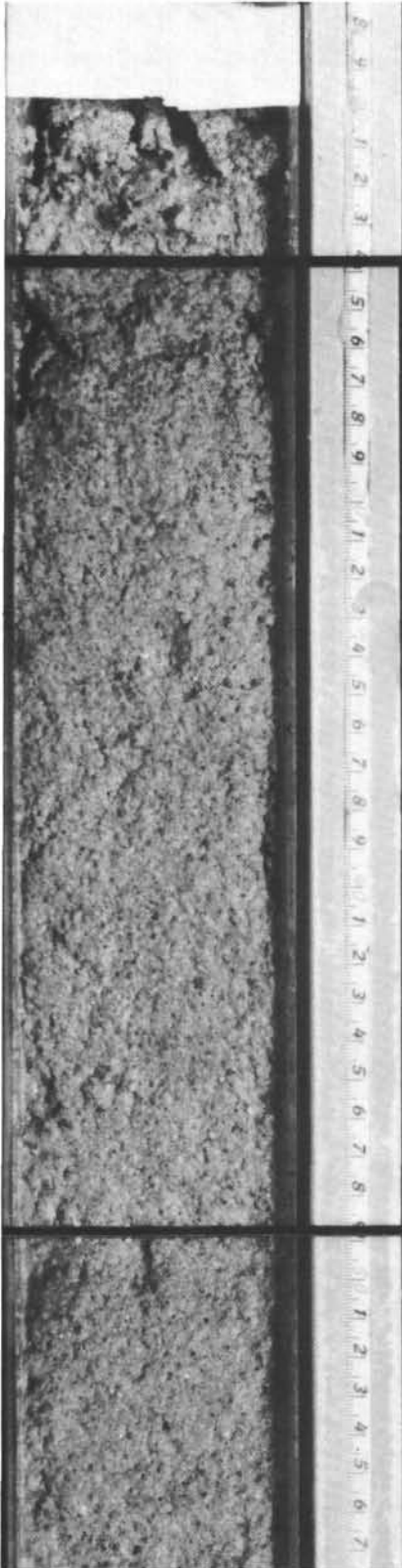


PLATE 3

Flysch, Laminites and Graded Beds.

- Figures 1, 2      241-28-3, 26-38 cm; 241-28-3, 2-13 cm. Laminites. Note discontinuity of bedding and possible subtle grading, Figure 2, 10-12 cm.
- Figure 3          241-28-1, 50-66 cm. Graded beds interbedded with laminites, 63.5-60.5 cm, 60.5-59 cm. Note burrowing 50-55 cm, and lamination 58-59 cm which seems to grade upward to finer sediment.
- Figure 4          241-28-1, 84-100 cm. Graded beds. Note sharp and apparently erosional base at 93 cm with associated rip-up clasts.

PLATE 3

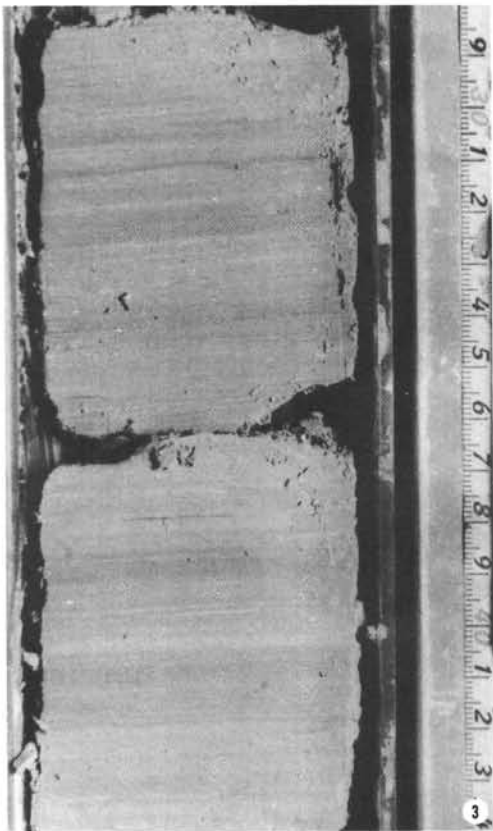
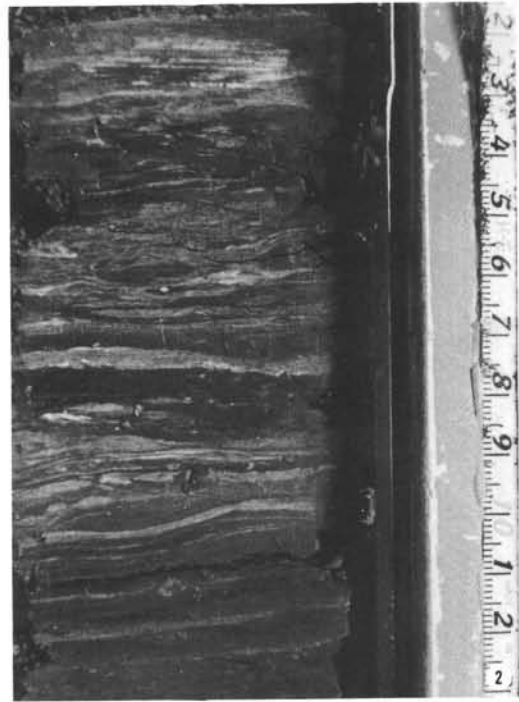
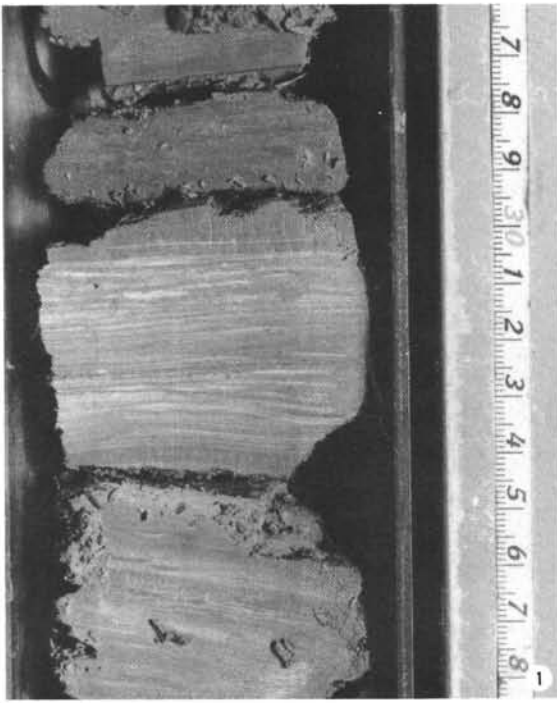


PLATE 4

Graded Beds (thin sections).

- Figure 1 239-1-1, 100 cm (plain light, width of view 0.75 mm). Siliceous sponge spicule with other silicate, oxide and biogenous detritus.
- Figure 2 241-10-4, 90-92 cm (plain light, width of view 0.75 mm). Graded bed showing quartz (Q), feldspar (Fs), foraminifera (F) and green hornblende (H) in dark matrix comprised of clay, coccoliths, and secondary pyrite.
- Figure 3 241-10-4, 90-92 cm (plain light, width of view 0.25 mm). Close-up of green hornblende with quartz, feldspar, and coccolith-clay matrix.
- Figure 4 240-1-3, 40-41 cm (plain light, width of view 0.75 mm). Biogenic graded bed predominantly composed of radiolarians (R), sponge spicules (S) and foraminifera (F).
- Figure 5 240-3-1, 28-29 cm (plain light, width of view 0.75 mm). Foraminifera filled with pyrite from biogenic graded bed.

PLATE 4

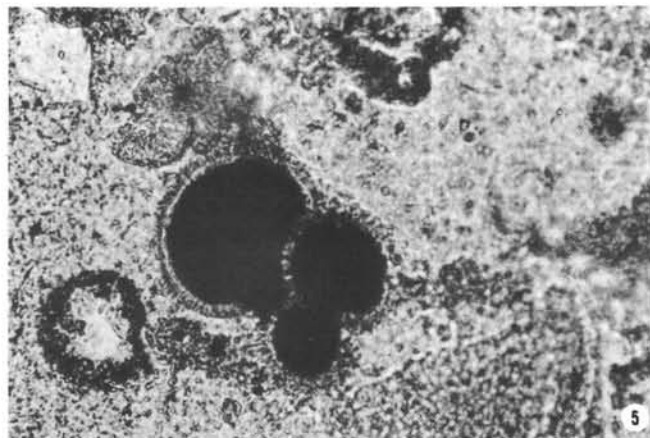
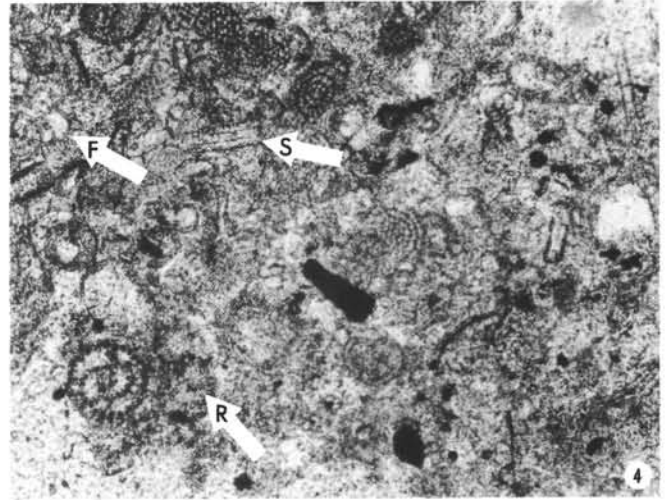
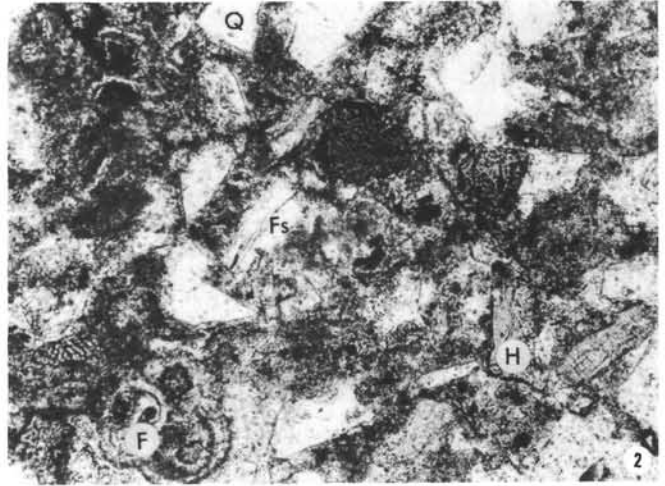
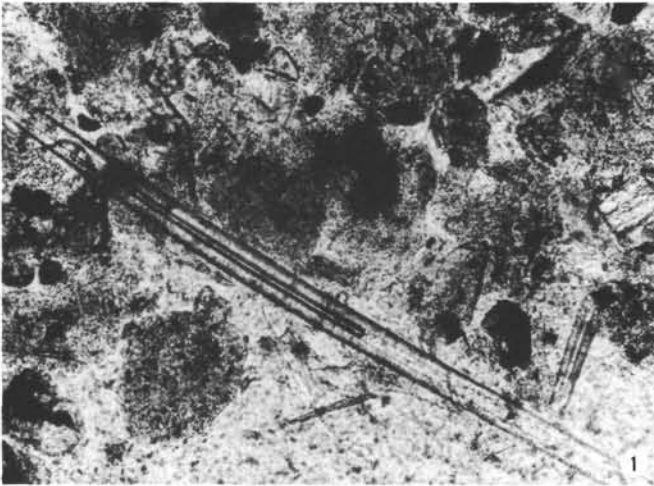
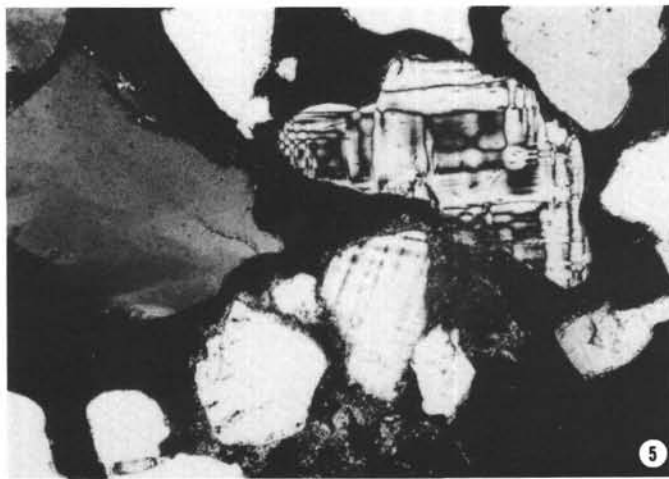
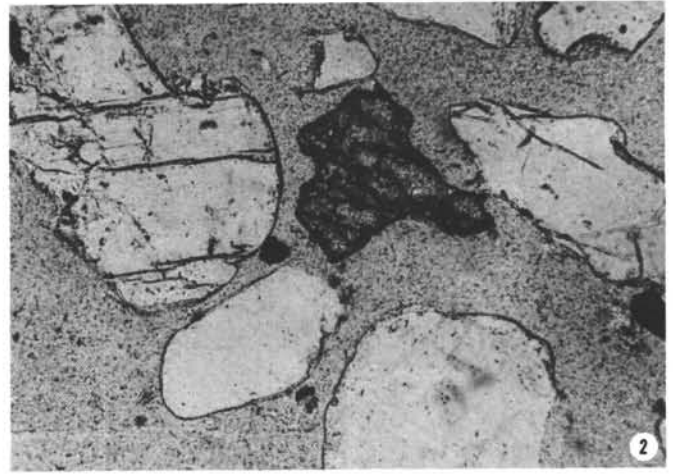
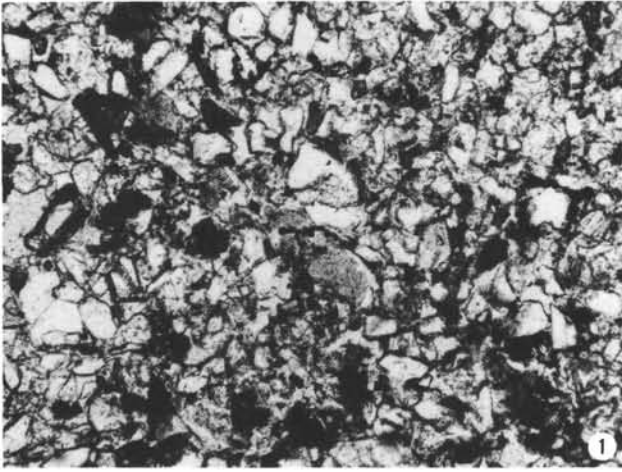


PLATE 5

Massive Sands (thin sections).

- Figure 1 240-4-2, 21-22 cm (plain light, width of view 3 mm). Unwashed massive sand, illustrating predominance of silicate grains.
- Figure 2 248-8-1, 119-121 cm (plain light, width of view 1 mm). Grain mount of massive sand showing garnet (high relief mineral, center) microcline (cleaved mineral, left) and quartz.
- Figure 3 244-1, CC (crossed nicols, width of view 3 mm). Granule size granitic fragment predominantly composed of microcline with included plagioclase quartz (plagioclase almost totally altered to calcite).
- Figure 4 243-1-1, 135-136 cm (crossed nicols, width of view 2.5 mm). Large (2 mm) strained composite quartz grain.
- Figure 5 240A-2-1, 99-100 cm (crossed nicols, width of view 3 mm). Microcline and quartz of massive sand. Note low birefringence matrix surrounding grains in lower center portion of figure.

PLATE 5



## PLATE 6

## Flysch Sandstones and Calcarenites, Site 241 (thin sections)

- Figure 1      241-27-2, 122-128 cm (plain light, width of view 0.9 mm). Calcarenite dominated by a linear skeletal fragment (bivalve?) and spheres comprised of fibrous radial calcite.
- Figure 2      241-27-2, 122-128 cm (plain light, width of view 0.25 mm). Close-up of fibrous radial calcite spheres suggests presence of distinct exterior wall and spar possibly replacing fibrous calcite. These spheres are probably foraminifera (*Orbulina?*) filled with secondary radial calcite; they are not oolites.
- Figure 3      241-29-2, 10-12 cm (plain light, width of view 0.8 mm). Calcareous sandstone showing dolomite replacing quartz grains.
- Figure 4      241-29-1, 10-12 cm (crossed nicols, width of view 0.8 mm). Close-up of quartz grain which is partially replaced by dolomite. Note how the polarized light emphasizes the relatively large crystal domains between silicate grains.
- Figure 5      241-28-2, 67-68 cm (plain transmitted light plus reflected light, width of view 3 mm). Elongate pyrite grains are predominantly opaque but show bright spots due to reflected light. The irregular pyritized areas probably were originally plant fragments.

PLATE 6

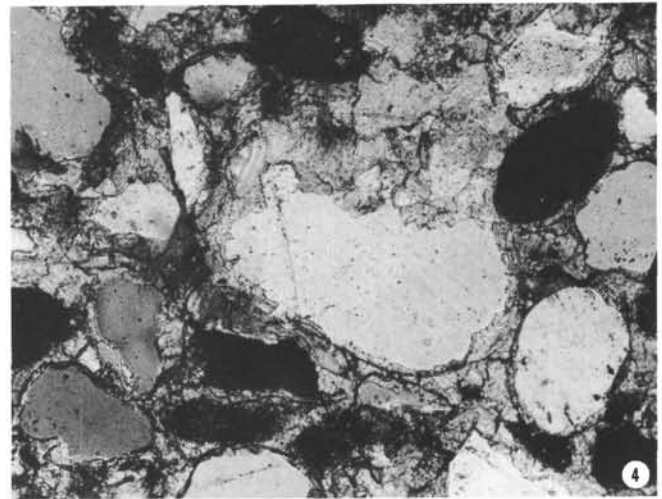
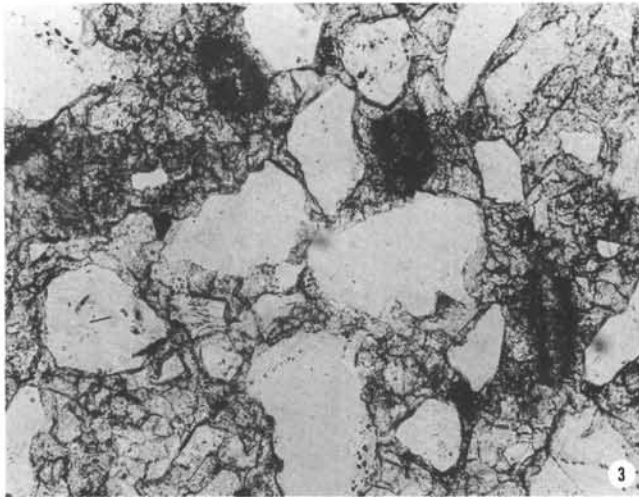
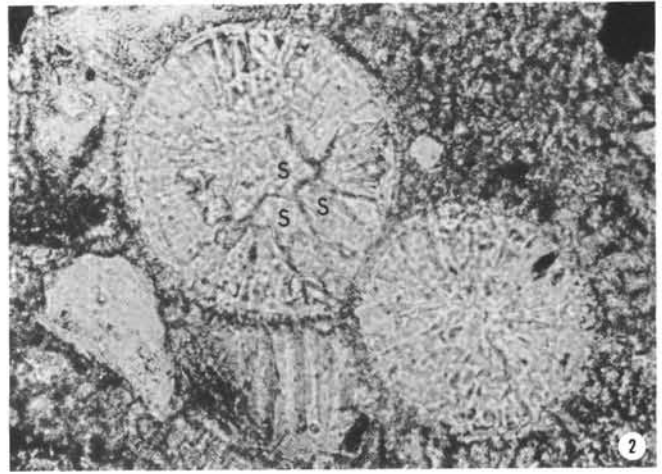
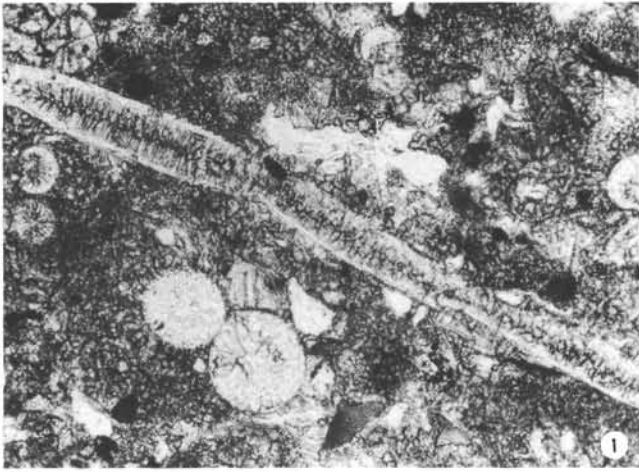


PLATE 7

Flysch: Massive Sandstone and Graded Beds.

- Figure 1      241-28-1, 101-145 cm. Massive sandstone. Note mudstone beds above and below as well as rip-up clasts incorporated in upper portions of beds (see grain-size analysis Figure 7).
- Figures 2,3    241-27-21, 25-36 cm; 241-27-3, 104-115 cm. Graded beds with distinct laminated bases. Top not well defined in bed of Figure 2 but apparently shown by color change in Figure 3, 116-117 cm.

PLATE 7

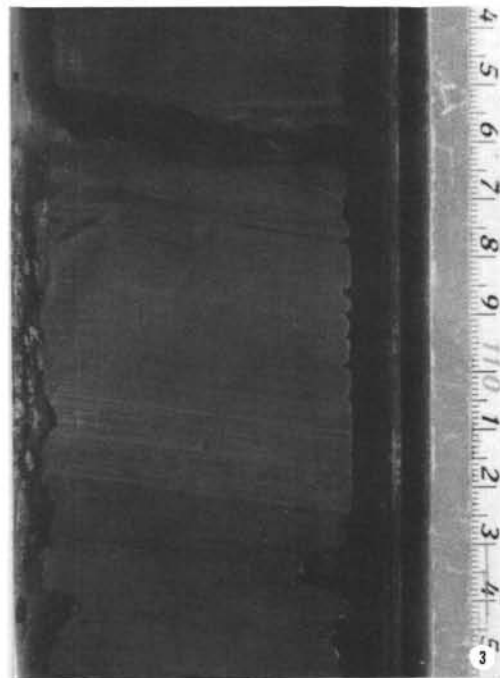
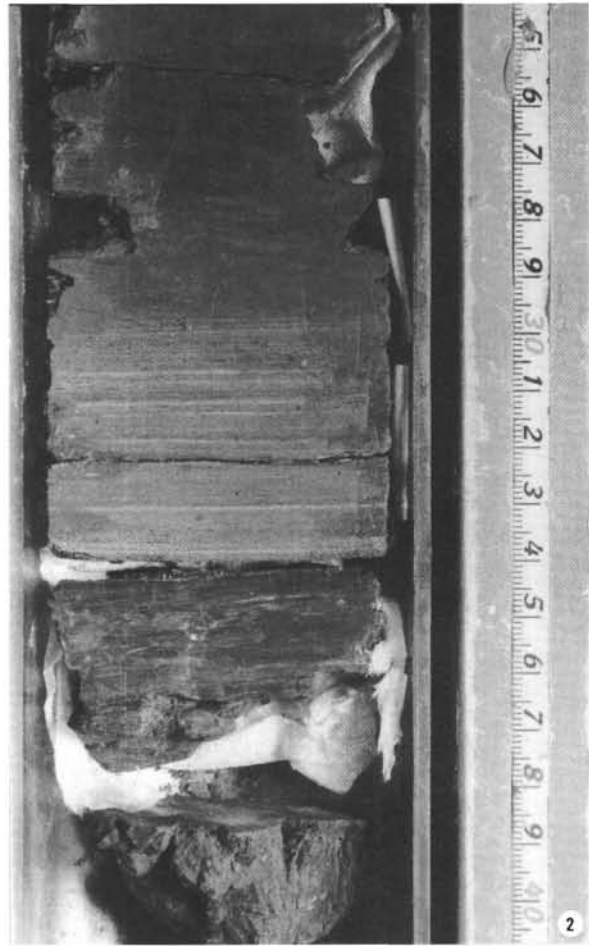


PLATE 8

Flysch Sandstones.

- Figure 1      Cross-bedded calcareous sandstone.
- Figure 2      241-28-2, 61-76 cm. Carbonaceous sandstone with 2% organic carbon remaining, much of original matter replaced by pyrite (see Plate 3, Figure 5).
- Figure 3      241-26-2, 3-23 cm. Slump folds passing upward into graded bed. Note overturned cross bedding at 20 cm.
- Figure 4      241-27-2, 121-135 cm. Though broken by drilling, this section apparently preserves complete Bouma Sequence: A-massive interval (132-134 cm), lower B-interval of parallel lamination (131-132 cm), C-convolute lamination (125-129 cm), D-upper interval of parallel lamination (123-125 cm), E-pelitic interval (121.5-123 cm).

PLATE 8

